



## OPEN ACCESS

EDITED BY  
Jia-Xi Zhou,  
Yunnan University, China

REVIEWED BY  
Huan Li,  
Central South University, China  
Chuanwei Zhu,  
Institute of Geochemistry (CAS), China  
Zhilong Huang,  
Institute of Geochemistry (CAS), China

\*CORRESPONDENCE  
Yuzhao Hu,  
✉ yuzhaohu@kust.edu.cn  
Yong Cheng,  
✉ cheng\_yong1988@163.com

SPECIALTY SECTION  
This article was submitted to  
Geochemistry,  
a section of the journal  
Frontiers in Earth Science

RECEIVED 27 November 2022  
ACCEPTED 30 December 2022  
PUBLISHED 13 January 2023

CITATION  
Xu S, Hu Y, Cheng Y, Zhu J, Ping Y, Zhang Q  
and Pei Z (2023), Genetic relationship  
between the Maoping Pb–Zn deposit and  
paleo-oil reservoir in the northern  
Yunnan–Guizhou depression: Evidence  
from bitumen trace elements and the *in-  
situ* sulfur isotope of pyrite associated  
with bitumen.  
*Front. Earth Sci.* 10:1109112.  
doi: 10.3389/feart.2022.1109112

COPYRIGHT  
© 2023 Xu, Hu, Cheng, Zhu, Ping, Zhang  
and Pei. This is an open-access article  
distributed under the terms of the [Creative  
Commons Attribution License \(CC BY\)](https://creativecommons.org/licenses/by/4.0/).  
The use, distribution or reproduction in  
other forums is permitted, provided the  
original author(s) and the copyright  
owner(s) are credited and that the original  
publication in this journal is cited, in  
accordance with accepted academic  
practice. No use, distribution or  
reproduction is permitted which does not  
comply with these terms.

# Genetic relationship between the Maoping Pb–Zn deposit and paleo-oil reservoir in the northern Yunnan–Guizhou depression: Evidence from bitumen trace elements and the *in-situ* sulfur isotope of pyrite associated with bitumen

Saihua Xu<sup>1</sup>, Yuzhao Hu<sup>1\*</sup>, Yong Cheng<sup>1,2\*</sup>, Jizhan Zhu<sup>1</sup>, Yuan Ping<sup>1</sup>,  
Qimeng Zhang<sup>1</sup> and Zixuan Pei<sup>1</sup>

<sup>1</sup>Faculty of Land and Resource Engineering, Kunming University of Science and Technology, Kunming, Yunnan, China, <sup>2</sup>Faculty of Metallurgy and Mining Engineering, Kunming Metallurgy College, Kunming, Yunnan, China

The coexistence of numerous Mississippi Valley-type (MVT) Pb–Zn deposits and oil/gas reservoirs in the world demonstrates that a close genetic link between them. The northern Yunnan–Guizhou depression (NYGD) is a tectonic unit containing Pb–Zn deposits, paleo-oil reservoirs and shale gas. However, previous studies on the relationship between hydrocarbon accumulation and Pb–Zn mineralization have been ignored. The Maoping Pb–Zn deposit is a large-sized MVT deposit in the NYGD where a large amount of solid bitumen (i.e., a paleo-oil reservoir) occurs, and it is an ideal area to study the relationship between hydrocarbon accumulation and lead–zinc mineralization. In this paper, the bitumen and pyrite associated with bitumen from the Xujiashai (discovered in this study) and Xiaocaoba paleo-oil reservoirs and the Maoping Pb–Zn deposit are researched. Geological observation has revealed that bitumen occurs in dissolution pores, fractures and intercrystalline pores in dolomite of the Upper Devonian and Carboniferous. The bitumen from Xujiashai, Maoping and Xiaocaoba with high and similar Raman equivalent reflectance ( $R_{mc}Ro\%$ ) indicates they are in over-mature level and may be derived from the cracking of early-accumulated crude oils. The bitumen in the Xujiashai paleo-oil reservoir and Maoping deposit has an abundant Pb and Zn content, indicating petroleum liquids may act as the transporting agents of metallogenic metal elements, carrying them to sites where mineralization may take place. The source rocks may have provided not only the oil for paleo-oil/gas reservoirs, but also a portion of ore metals for the Pb–Zn mineralization. The bacterial sulfate reduction (BSR) and thermochemical sulfate reduction (TSR) processes were recorded by the pyrite in the paleo-oil reservoir, which was consistent with the mechanism of reduced sulfur formation in the Maoping deposit. In addition, the large negative ( $-27.7\%$  to  $-5.7\%$ ) and positive ( $0.9\%$  to  $19.2\%$ )  $\delta^{34}S$  values of the pyrite associated with the bitumen in the paleo-oil reservoir were similar to those of the sulfide in the Maoping deposit. We believe that the formation and evolution of the paleo-oil reservoirs are closely related to the metallogenic process of the Maoping

Pb–Zn deposit, and the sulfides in them have the same sulfur source and formation mechanism as reduced sulfur. BSR phenomena could occur in prior to migration of the hydrocarbons into the reservoir or low mature oil stage in paleo-oil reservoir; a small amount of  $H_2S_{BSR}$  was combined with metal ions in ancient oil reservoirs and deposits to form early subhedral, xenomorphic granular, fine-grained strawberry aggregate pyrite and/or gelatinous sphalerite. The paleo-gas reservoir formed by the evolution of the paleo-oil reservoir in the main metallogenic period potentially participated in the mineralization; that is, organic gas acted as a reducing agent and transformed  $SO_4^{2-}$  in the upper Devonian Zaige Formation gypsum strata on the periphery of the Maoping lead–zinc mining area into  $H_2S_{TSR}$  through TSR, providing reduced sulfur and creating the environmental conditions for mineralization. During or after the transformation of the paleo-oil reservoir to a paleo-gas reservoir, the decoupling of metals and organic complexes may have provided the ore metals for mineralization. Massive sulfide precipitation may have occurred during or after the paleo-oil reservoir cracked into the paleo-gas reservoir.

#### KEYWORDS

paleo-oil reservoir, bitumen trace element, *in-situ* sulfur isotope, Maoping deposit, northern Yunnan–Guizhou depression

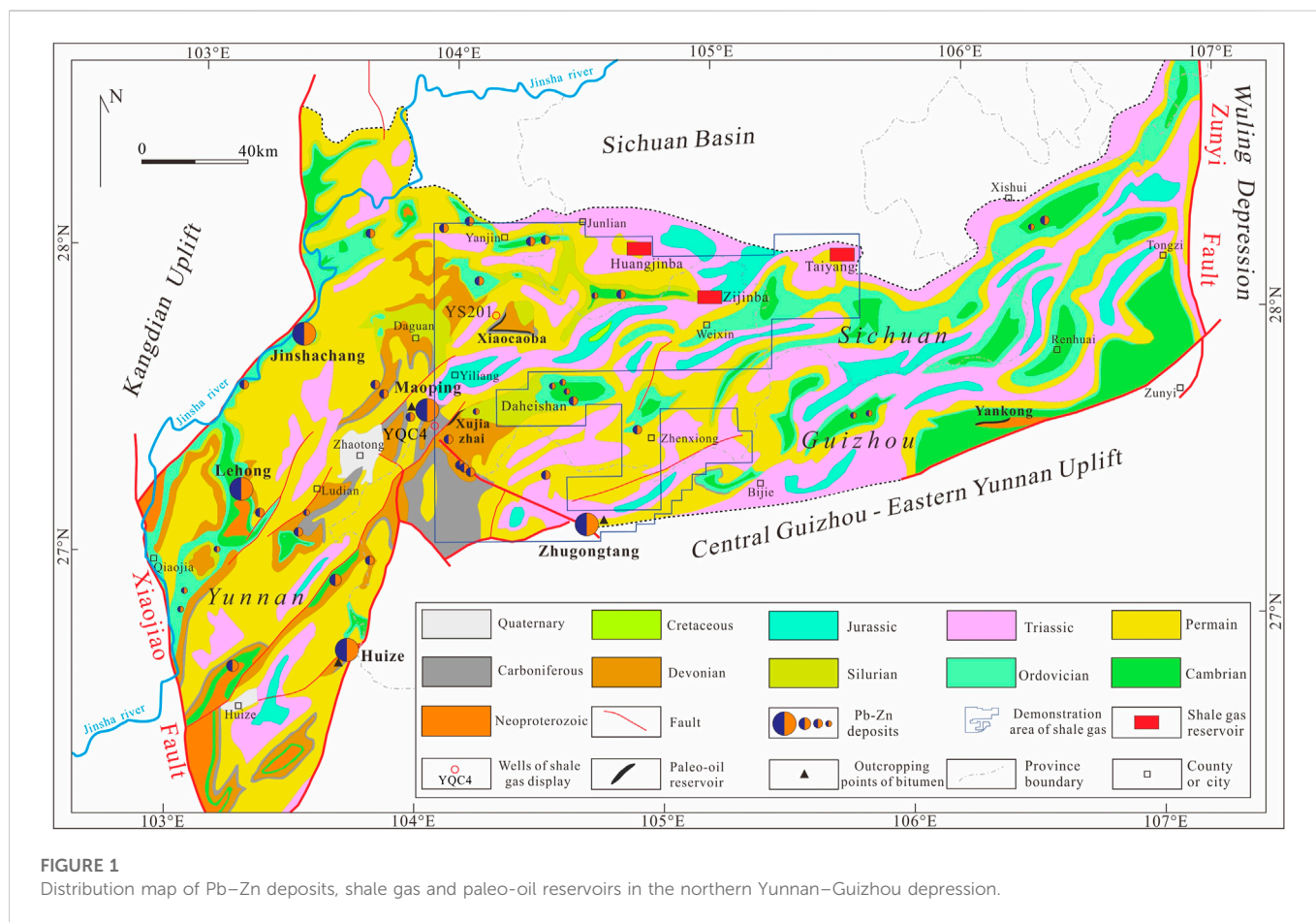
## 1 Introduction

In many cases, hydrocarbons migrate separately from or together with the mineralizing fluids within sedimentary basins and are deposited in the form of petroleum or solid bitumen in the vicinity of sulfides (Püttmann et al., 1988; Manning and Gize, 1993; Kozłowski et al., 1995; Spangenberg and Herlec, 2006; Rieger et al., 2008; Williford et al., 2011; Lan et al., 2021). Therefore, at present, a common phenomenon is that many lead–zinc deposits in the world are closely paragenetic or spatially associated with oil and gas reservoirs (Kesler et al., 1994; Lin, 1995; Sicree and Barnes, 1996; Chen et al., 2008; Wu et al., 2013a; Fang et al., 2016; Huang et al., 2019; Huang et al., 2021; Lan et al., 2021; Wang et al., 2022). The closely spatial connection between Pb–Zn deposits and paleo-oil reservoirs and the development of high precision testing technology has added to the deeply research on the relationship between organic matter (crude oil, solid bitumen, methane and/or ethane, etc.) and mineralization, creating a hot spot in the study of mineral deposits (Li et al., 2021). Oil and gas can actively participate in the mineralization of metal deposits and play an important role in the formation of ore deposits, which primarily as follows: 1) the preenrichment of metals (Chen et al., 2002); 2) activation, migration and enrichment of metallogenic elements (Girodano, 1985; Liu et al., 2000; Li et al., 2002; Saintilan et al., 2019; Sanz-Robinson and Williams-Jones, 2019); 3) provides a large amount of reduced sulfur ( $H_2S/HS^-$ ) for mineralization (Gu et al., 2012; Cheng et al., 2021; Huang et al., 2021; Wang et al., 2022); 4) organic acids are produced to dissolve carbonate rocks to provide ore storage space, and organic carbon is provided to participate in the precipitation of hydrothermal carbonate (Liu and Zheng, 2000; Liu et al., 2016); 5) to create the physical and chemical conditions necessary for mineralization (Liu et al., 2000).

The northern Yunnan–Guizhou depression (NYGD) is a tectonic unit that incorporates Pb–Zn deposits, paleo-oil reservoirs and shale gas (Figure 1); it is located South of the Sichuan Basin and coincides with the eastern part of the famous Sichuan–Yunnan–Guizhou lead–zinc ore concentration area, including the Huize, Maoping, Lehong, Zhugongtang, Jinshachang super-large lead–zinc deposits and many medium–small lead–zinc deposits (Figure 1). Bitumen can be observed in most of these deposits. In recent years, the

Yankong (Yang et al., 2012; Bao et al., 2016), Xiaocaoba (Bao et al., 2016; Zhang et al., 2017) and Xujiazhai (a new discovery in this study) paleo-oil reservoirs were successively discovered in the area. However, the genetic relationship between them and the lead–zinc deposits in the area has not been studied. The Maoping deposit is not only one of the richest MVT lead–zinc deposits in the area and in the world, but also existence of abundant solid bitumen compared with other deposits in NYGD. Solid bitumen is spatially closely related to the ore. Meanwhile, liquid phase  $C_2H_6$  organic matter and  $CH_4$ ,  $C_2H_6$ ,  $C_6H_6$  organic gas were found in a fluid inclusion study (Han et al., 2019), showing the formation and evolution of oil may be close genetic link to lead–zinc mineralization. Hence, it is an ideal area to study the relationship between organic matter and lead–zinc mineralization. Although our predecessors made efforts to identify some possible roles that organic matter may play in the genesis of the Maoping deposit (Han et al., 2007; Wei, 2011; Ren, 2018; Yang et al., 2019), the source of the organic matter (bitumen,  $CH_4$ ,  $C_2H_6$ , etc.) is not well been constrained, along with whether it is genetically related to mineralization and how it participated in the mineralization. The lack of such information has severely limited our ability to understand the role of organic matter in the formation of Maoping deposit.

Previous works on this MVT Pb–Zn mineralization were focused mainly on the ore fluids and ore-material source (Zou et al., 2004; Han et al., 2007; Tan et al., 2019). Han et al. (2007) proposed that the ore-forming fluid was the compositing results of the magma water, metamorphic and hosted water, and mainly derived from magmatic hot fluid and hosted formation water. Tan et al. (2019) considers that the Maoping large-scale Pb–Zn deposit is the product of fluid mixing. Other studies explored on the possible sulfur source from seawater sulfates (Tan et al., 2019; Yang et al., 2019), which have shown reduced sulfur was mainly supplied by the thermochemical sulfate reduction (TSR) and bacterial sulfate reduction (BSR), and the lead source from ore-bearing sedimentary rocks and underlying basement rocks (Tan et al., 2019; He et al., 2020). Many studies have shown that petroleum is rich in ore-forming metals, and it could potentially be a carrier of both ore-forming metals and ore-forming fluids (Peabody and Einaudi, 1992; Manning and Gize, 1993; Zhuang and Lu, 1996). For the bitumen-rich Maoping deposit, it is unclear



whether petroleum was a carrier of ore metals as the ore-forming fluid or was unrelated to the Pb–Zn mineralization. Besides, for the MVT deposit with abundant bitumen, previous studies explained only the source and formation mechanism of reduced sulfur according to the sulfur isotopes of sulfide in the deposit. Sulfide is also commonly found in paleo-oil reservoir. The comparison of sulfur isotope of sulfide in paleo-reservoir and ore deposit may provide certain information for the formation of ore deposit. In fact, the comparative studies of sulfur isotopes between sulfide in the deposit and the sulfur isotopes of sulfide in the paleo-oil reservoir are rarely conducted. This may be attributed to the fact that sulfides in paleo-oil reservoirs are usually small, led to traditional S isotope test methods are limited. Therefore, in this paper, *in-situ* sulfur isotopes of the pyrite associated with bitumen in the Xujiazhai and Xiaocaoba paleo-oil reservoirs were studied, and the material source of the Maoping deposit were discussed through bituminous trace elements, aimed to revealing the relationship between the paleo-oil reservoir and lead–zinc mineralization in the Maoping deposit.

## 2 Regional geologic setting of the northern Yunnan–Guizhou depression

The NYGD, comprising about 39,800 km<sup>2</sup> (Figure 1), is located on the margin of Sichuan, Yunnan, and Guizhou provinces and is bounded by the Zunyi fault. It lies adjacent to the Wuling depression in the East, with the Xiaojiao fault as a dividing line in

the West, and is adjacent to the Kangdian uplift. It borders on Sichuan Basin in the North and is connected with the central Guizhou–eastern Yunnan uplift in the South.

The northern Yunnan–Guizhou area experienced the tectonic and sedimentary evolution history of the late Proterozoic to early Paleozoic, the late Paleozoic to middle Triassic and the Mesozoic, and developed the marine Sinian–middle Triassic and continental upper Triassic to lower Cretaceous sedimentary assemblages with complete stratigraphy, great thickness and wide distribution. At present, the sedimentary caps in northern Yunnan–Guizhou are characterized by a strong compressive structure, which is a typical trough-like folded deformation belt with a gentle broad anticline and steep narrow syncline. The tectonic deformation intensity lies between the trough-like fold deformation in the southern margin of Sichuan Basin and the thrust fold deformation in southeastern Guizhou. The tectonic strikes are mainly NS-, NEE- and NE-trending, and the anticlinal belt and synclinal belt show a northwest convex arc in the eastern Weining-Bijie. From the central Guizhou–eastern Yunnan uplift to the northern Yunnan–Guizhou depression to the Sichuan Basin, the tectonic deformation moves from strong to weak, indicating that the study area has been affected by the continuous intracontinental orogeny of Jiangnan and Xuefeng since the Yanshanian and by the northward thrust and extrusion of the Indian plate during the Himalayan period.

There are three sets of source and reservoir assemblages in the NYGD: 1) black mudstones of the lower Cambrian Qiongzhusi Formation and dolomite of the lower Cambrian Longwangmiao

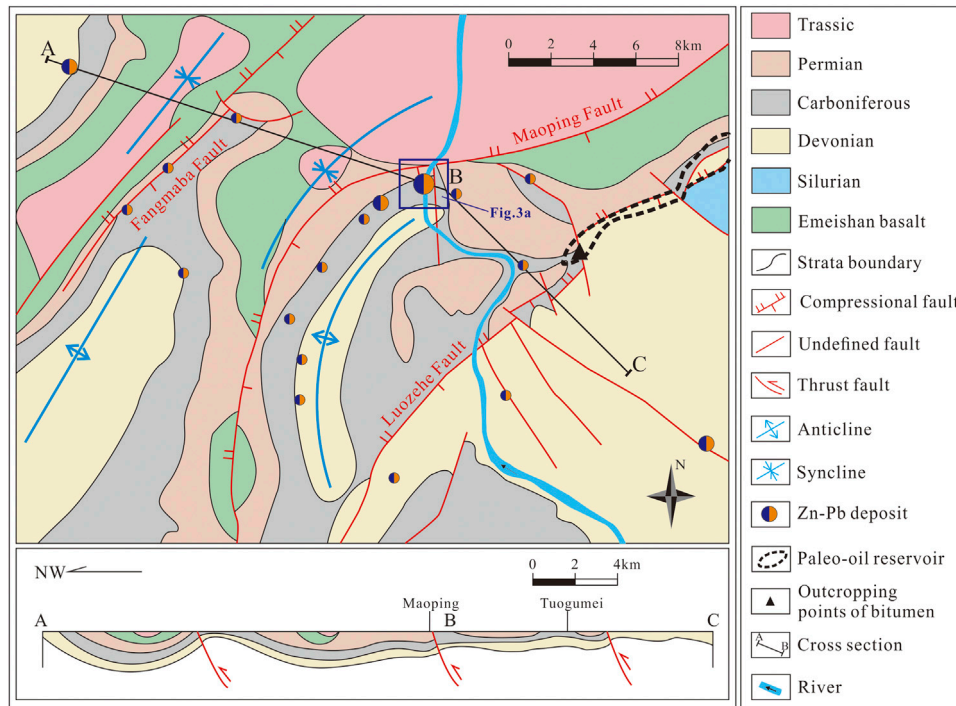


**FIGURE 2**  
Geological map of the Maoping district showing the stratigraphy, structure and distribution of Pb–Zn deposits (modified after Liu and Lin, 1999).

Formation; 2) black mudstones of the Ordovician Wufeng Formation and Silurian Longmaxi Formation and carbonate rocks of the Upper Devonian and Carboniferous; 3) black mudstones of the Carboniferous Wanshoushan Formation and Carboniferous carbonate rocks. High-quality source rocks of the Wufeng Formation and Longmaxi Formation in northern Yunnan–Guizhou have a TOC (total organic carbon) content of 1.5%–3.5%, thickness of 50–350 m, and distribution area of 11,100 km<sup>2</sup>. The thickness of high-quality Cambrian source rocks is 120–500 m, and the distribution area is 31,600 km<sup>2</sup>, indicating strong oil generation potential (Liang et al., 2011). Three sets of source rocks in the areas are also shale gas occurrence beds, and the current exploration and development beds are the Wufeng Formation and Longmaxi Formation. According to incomplete statistics, since 2009, 2D and 3D seismic exploration engineering has covered 2,661 km and 121 km<sup>2</sup>, respectively, and 106 wells have been drilled (China National Petroleum Corporation internal information). At present, the proved reserves are more than  $1,000 \times 10^8$  m<sup>3</sup>, and the shale gas production capacity of  $18 \times 10^8$  m<sup>3</sup>/a has been achieved (including the Zijinba gas field in Yunnan province, the Huangjinba and Taiyang gas field in Sichuan province, Figure 1; Liang et al., 2020; Du et al., 2021).

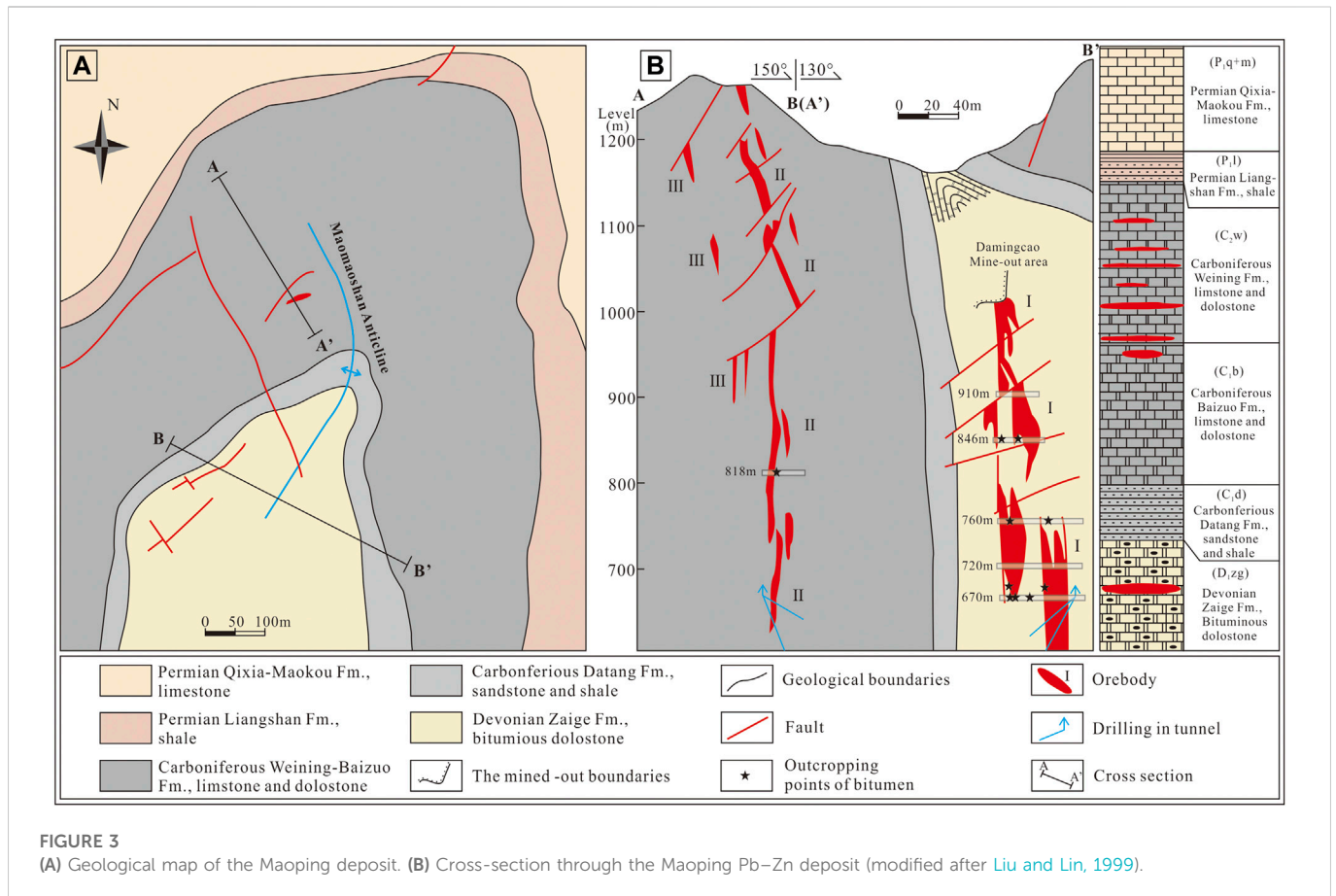
### 3 Geology of the Maoping Pb–Zn deposit

Within the mining district, Silurian, Devonian, Carboniferous, and Permian are mainly exposed, and their contact relationship between the strata is disconformable (Figure 2). The Silurian strata consist of shale, sandstone, and argillaceous sandstone. The lower

Devonian strata comprise sandstone, mudstone, and dolostone and overlie the Devonian Zaige Formation bituminous dolostone. The strata of the lower Carboniferous Datang and Baizuo Formations are composed of limestone with a thin layer of shale and a dolostone interlayer with ~3 m thick clay shale, respectively. The middle Carboniferous Weining Formation conformity overlies the lower Carboniferous Baizuo Formation and mainly consists of limestone and dolostone. The lower Permian Liangshan Formation comprises shale and sandstone and overlies the lower Permian Qixia and Maokou Formations limestone. Additionally, the Emeishan flood basalts are widespread outside of the mining area.

The structures in the Maoping mining area are mainly NE- and NW-trending. The NE-trending structures are arranged successively from NW to SE, including the Fangmaba compressional fault, Maoping compressional fault, Luozehe compressional fault, and Maomaoshan inverted anticline. Specifically, the Maoping fault has a strike of NE10°–80° and a dip of SE65°–85° and is 30 km long. The Luozehe fault strikes NE30°–40° and dips steeply at SE65°–70° with a length of >40 km. The Fangmaba fault strikes NE25° and dips SE67°–85° with a length of >20 km. The fold axis of the Maomaoshan inverted anticline has a variable strike: NW350° in its western limb and NE20°–45° in its northern wing. Its western wing is overturned with a dip of 65°–86°, while the eastern wing has a relatively gentle dip (17°–35°). The Maomaoshan inverted anticline and Maoping compresso-shear fault are mainly ore-control structures (Figures 2, 3A).

Sulfide orebodies at Maoping occur as steeply plunging and pipe-shaped and are mainly hosted within the overturned NW limb of the Maomaoshan anticline. Post-ore NW-trending faults suggest that the



sulfide orebodies are weak deformations rather than metamorphisms. Individual pipes have been grouped into three larger orebodies, including Orebody I, Orebody II, and Orebody III (Figure 3B). Orebody I is the largest, hosted within the Devonian Zaige Formation, which has a length of 280–320 m, width of 5–34 m, and 800 m in thickness with average ore grades of 13.0 wt.% Zn, 7.5 wt.% Pb, and 135 g/t Ag. Orebody II is hosted within the lower Carboniferous Baizuo Formation, and is 20–182 m long, 22 m wide, and 540 m thick with average ore grades of 16.0 wt.% Zn and 6.0 wt.% Pb (Wei et al., 2021a). Orebody III is hosted within the interformational faulted zone of the lower Carboniferous Weining Formation. The orebody is 43–202 m in length, 5 m in width, and 170 m in thickness with average ore grades of 7.6 wt.% Zn and 9.0 wt.% Pb.

The ore mineral assemblage of the Maoping deposit is simple. The ore minerals are mainly sphalerite, galena and pyrite, with a small amount of marcasite, arsenopyrite, chalcopyrite, and siderite. The gangue minerals are mainly dolomite, calcite, bitumen, and a small amount of quartz. Wall rock alterations in Maoping are principally dolomitization and calcitization, which are closely associated with Pb–Zn mineralization.

Tunnel survey discovered that the Maoping paleo-oil reservoir almost overlaps with the largest orebody (No. I-6) (Figure 4). Bitumen is extensively distributed in both Hexi and Hedong ore blocks in the Maoping deposit. Bitumen is commonly associated with metal sulfides, dolomite, calcite and quartz (Figures 5A–F). Bitumen cutting through the wall rocks means that the bitumen is not the product of the sedimentary rock formation period (Figure 5G). Some

are distributed in the edges of metal minerals, and others are encased by metal minerals (Figures 5H–K), indicating that the bitumen is formed before or almost at the same time as mineralization. Some bitumens also tightly filled between dolomite crystals in wall rocks (Figure 5L). Based on the previous research work (Wei, 2011) and this study, a paragenetic sequence for the Maoping deposit was developed (Figure 6).

### 4 Paleo-oil reservoir characteristics

The Xujiashai paleo-oil reservoir is located 5 km East of the Maoping lead–zinc deposit (Figures 1, 2), 12.5 km long from East to West and more than 3 m thick. The lithology of the reservoir is mainly medium–fine crystal dolomite. Bitumen occurs in dissolution pores and fractures of dolomites of the Upper Devonian and Carboniferous and dolomite intercrystalline pores (Figures 7A,A',B–D). Most of the dolomite intercrystalline pores are filled with bitumen, most fully filled and some half-filled (Figure 7E). Bitumen is black, granular, or disseminated, hard in texture, does not stain hands and has no fluorescence, exhibiting the characteristics of pyrobitumen. It is black under transmitted light, indicating a high degree of evolution. Pyrite is abundant in this paleo-oil reservoir, mostly with irregular or subhedral–xenomorphic (Figures 7F, G).

The Xiaocaoba paleo-oil reservoir is located about 40 km northeast of the Maoping lead–zinc deposit (Figure 1). Bioclasts have developed in the reservoir, mainly including sponges, coral, and archaeocyatha clasts. The lithology of the reservoir is primarily fine crystal dolomite and secondary

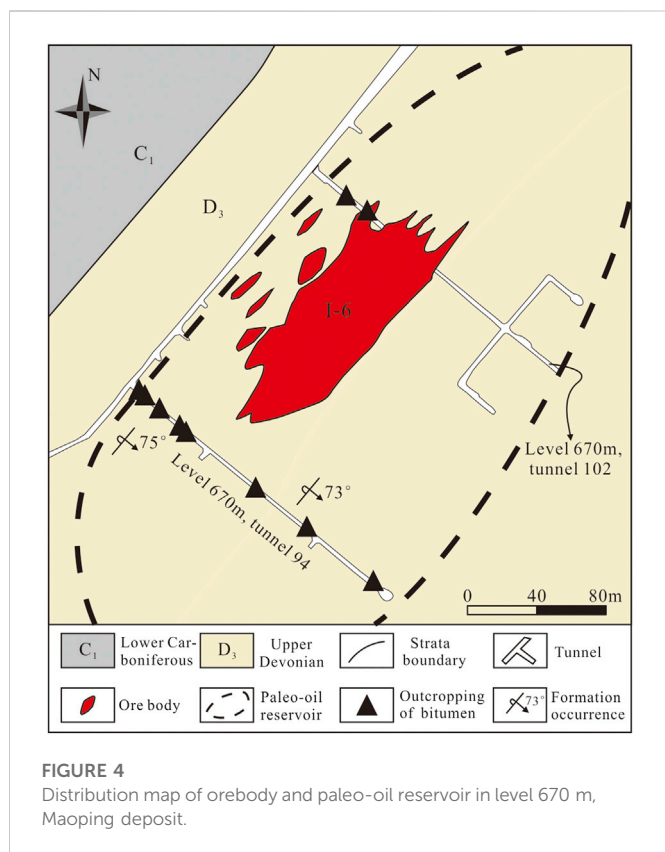


**FIGURE 4**  
Distribution map of orebody and paleo-oil reservoir in level 670 m, Maoping deposit.

medium crystal dolomite, and a small part is coarse-crystal dolomite. The matrix pores of the reservoir are mainly intergranular pores and intergranular dissolved pores. The porosity of the matrix is small, but dissolved pores and caves are very developed. Most of them were formed by the dissolution of biological coelom; their size is generally 3–5 cm, and some exceed 10 cm. Moreover, cracks and dissolution widening cracks are also more common. The pores and dissolution fractures are filled with bitumen and calcite. Most of the dolomite intercrystalline pores are fully filled with bitumen, some are half-filled, and they are disseminated or attached to the edge of dolomite crystal. Bitumen is concentrated in the upper Devonian, and the thickness of the reservoir is about 10 m at the minimum and close to 40 m at the maximum (Zhang et al., 2017). According to the distribution area, reservoir thickness, reservoir porosity, and bitumen degree of filling, the original reserves of the Xiaocaoba Devonian paleo-reservoir are estimated to be about  $6,000 \times 10^4$  t (Zhang et al., 2017). Pyrite exists in this paleo-oil reservoir, and most of it is distributed in bitumen with subhedral (Figure 7H), irregular (Figure 7I), and fine-grained aggregate strawberry (Figure 7J), with sizes ranging from 1 to 100  $\mu\text{m}$ . The strawberry pyrite partially oxidized to grayish goethite.

## 5 Samples and analytical methods

### 5.1 Samples

Bitumen samples were mainly collected from the Xujiashai and Xiaocaoba paleo-oil reservoirs and Maoping lead–zinc mining area. The pyrite closely associated with the bitumen of the Xujiashai and Xiaocaoba paleo-oil reservoirs was selected for *in-situ* sulfur isotope

analysis. Five bitumen samples were used for the analysis of trace elements in bitumen, of which three bitumen samples were collected from the Xujiashai paleo-oil reservoir and two bitumen samples from the Maoping deposit. To ensure the freshness of the analytical samples and minimize the contamination, the samples were treated as follows: the sample was cleaned and its edge was removed before crushing, and crushed samples for bulk bitumen analyses were separated and handpicked under a binocular microscope to ensure a purity of >99%. Then the samples selected under the binocular microscope were crushed to about 200 mesh with an agate mortar, and about 1–2 g sample powder was weighed for testing.

### 5.2 Analytical methods

#### 5.2.1 Laser Raman

The laser Raman spectrum analysis of bitumen was completed in the Laboratory of the Faculty of Land and Resources Engineering, Kunming University of Science and Technology. The RENISHAW inVia Raman microscope micro laser Raman spectrometer was used for the analysis, and the light source was a Spectra-Physics argon ion laser with a 514 nm laser wavelength and a 40 mW laser power. The laboratory temperature was 23°C and the humidity 35%.

#### 5.2.2 Trace elements

The analyses of trace elements were carried out at the Institute of Geochemistry, Chinese Academy of Sciences (Guangzhou). Trace elements were determined by a Jena Plasma Quant inductively coupled plasma mass spectrometry (ICP-MS) analyzer. About .0500 g of powdered sample was placed in a PTFE vessel, and .6 mL of HF and 3 mL of HNO<sub>3</sub> were added. The sealed vessels were then placed in an electric oven and heated to 185°C for about 36 h. After cooling, the vessels were heated on a hot plate to evaporate to dryness. A total of 200 ng of Rh was added as an internal standard, and then 2 mL of HNO<sub>3</sub> and 4 mL of water were added. The vessel was again sealed and placed in an electric oven at 135°C for about 5 h to dissolve the residue. After cooling, the final dilute factor was about 3,000 for ICP-MS measurement.

Analytical results and the uncertainties of reference materials, AMH-1 (andesite) and OU-6 (slate) agreed well with the reference values (Thompson et al., 2000; Potts and Kane, 2005). The accuracies of the ICP-MS analyses were estimated to be better than  $\pm 10\%$  (relative) for most elements.

#### 5.2.3 *In-situ* sulfur isotope

*In-situ* sulfur isotope analyses of pyrite were performed on a Neptune Plus MC-ICP-MS (Thermo Fisher Scientific, Bremen, Germany) equipped with a Geolas HD excimer ArF laser ablation system (Coherent, Göttingen, Germany) at the Wuhan Sample Solution Analytical Technology Co., Ltd., Hubei, China. In the laser ablation system, helium was used as the carrier gas for the ablation cell and was mixed with argon (makeup gas) after the ablation cell. The single spot ablation mode was used. Then the large spot size (44  $\mu\text{m}$ ) and slow pulse frequency (2 Hz) were used to avoid the down hole fractionation effect that was reported by Fu et al. (2016). One hundred laser pulses were completed in one analysis. A new signal-smoothing device was used downstream from the sample cell to efficiently eliminate the short-term variation of the signal, especially for the slow pulse frequency condition (Hu et al., 2015). The laser fluence was kept constant at  $\sim 5 \text{ J/cm}^2$ . The Neptune Plus was equipped with nine Faraday cups fitted with 1,011  $\Omega$

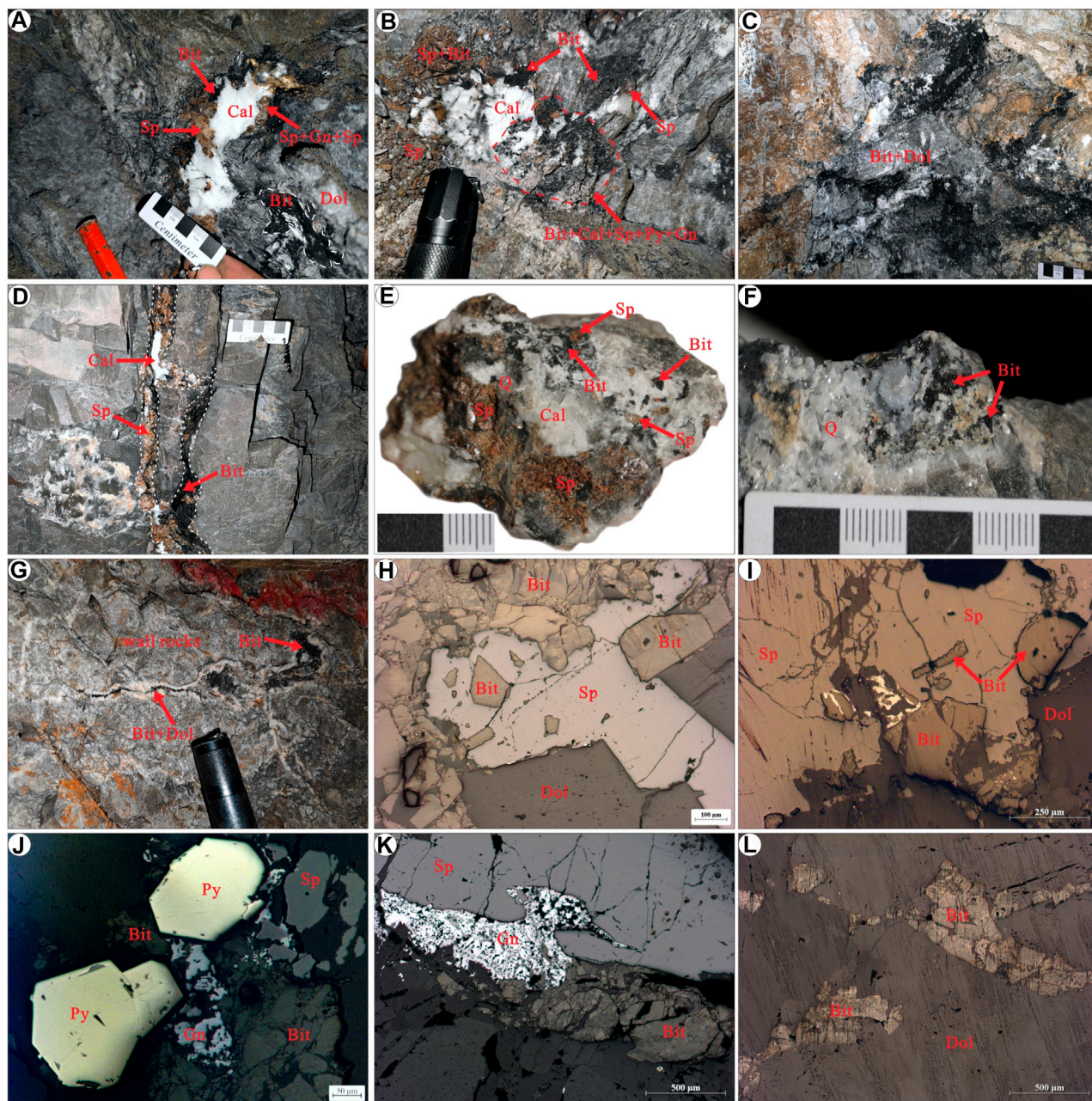


**FIGURE 5**  
 Photos of bitumen and ore in the Maoping deposit. (A,B) Bitumen in Devonian dolomite closely associated with sphalerite, a small amount of galena and coarse-grained calcite (Near orebody I-6, level 683 m, Hedong ore block, Maoping deposit); (C) Bitumen in the form of clumps or binder closely associated with dolomite (level 846 m, Hedong ore block, Maoping deposit); (D) Bitumen in Carboniferous dolomite; sphalerite, calcite and bitumen intermingling and filling in along the fissure (level 818 m, Hexi ore block, Maoping deposit); (E) Ore hand specimen, spherical bitumen coexists with sphalerite (Near orebody I-6, level 683 m, Hedong ore block, Maoping deposit); (F) Spherical bitumen filled between quartz crystals (level 670 m, Hedong ore block, Maoping deposit); (G) Bitumen in dolomite vein (level 670 m, Hedong ore block, Maoping deposit); (H) Yellowish-brown bitumen under the light reflected by the polarizing microscope, some of it coated by sphalerite, and some are distributed in the edges of sphalerite; (I) Yellowish-brown bitumen at the edge of sphalerite under the light reflected by the polarizing microscope; (J) Galena + sphalerite + pyrite + dolomite + bitumen symbiotic association; (K) Galena + sphalerite + dolomite + bitumen symbiotic association; (L) Yellowish-brown bitumen tightly filled between dolomite crystals. Cal, calcite; Dol, dolomite; Q, quartz; Sp, sphalerite; Gn, galena; Py, pyrite; Bit, bitumen.

resistors. Isotopes  $^{32}\text{S}$ ,  $^{33}\text{S}$ , and  $^{34}\text{S}$  were collected in Faraday cups using the static mode. The newly designed X skimmer cone and Jet sample cone in Neptune Plus were used to improve the signal intensity. Nitrogen (4 mL/min) was added to the central gas flow to reduce the polyatomic interferences. All measurements were performed using the medium resolution with a revolving power (as defined by a peak edge width of 5%–95% of the full peak height) that was always greater than 5,000.

A standard-sample bracketing method (SSB) was employed to correct for instrumental mass fractionation. To avoid the matrix effect, a pyrite standard PPP-1, a chalcopyrite standard GBW07268 (a pressed pellet), and a synthetic  $\text{Ag}_2\text{S}$  standard IAEA-S-1 (a pressed pellet) were chosen as reference materials for correcting the natural pyrite, pyrrhotite and pentlandite samples, the natural chalcopyrite samples, and the natural  $\text{Ag}_2\text{S}$  samples, respectively. The reference

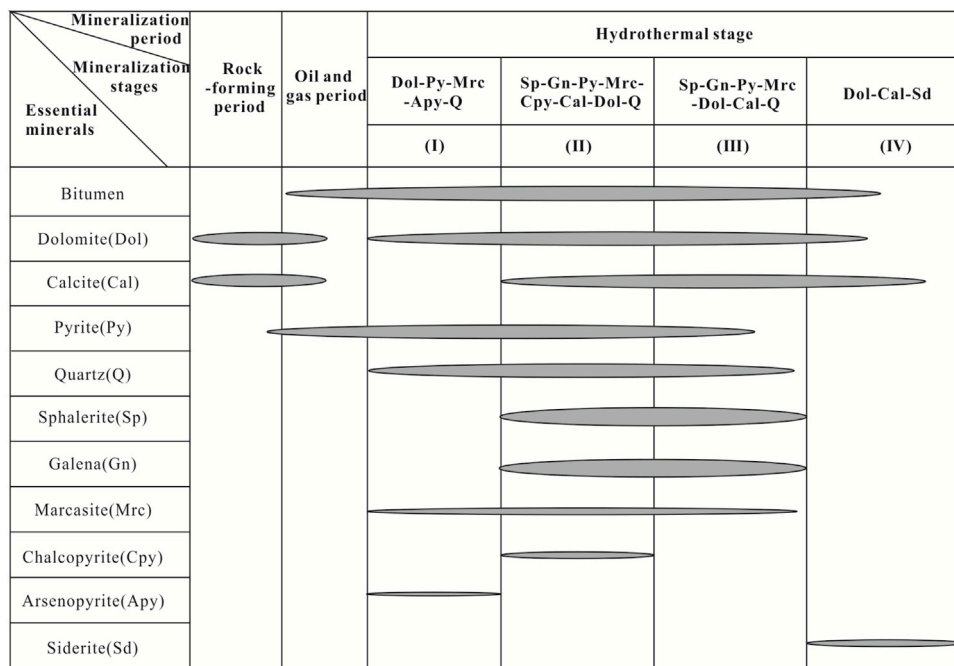


**FIGURE 6**  
The mineralization stages and the mineral arisen sequence in Maoping Pb-Zn deposit.

values of  $\delta^{34}S_{V-CDT}$  in these standards were reported by Fu et al. (2016). In addition, the in-house references of a pyrrhotite SP-Po-01 ( $\delta^{34}S_{V-CDT} = 1.4 \pm .4$ ), a chalcopyrite SP-CP-01 ( $\delta^{34}S_{V-CDT} = 5.45 \pm .3$ ), and two synthetic  $Ag_2S$  standard IAEA-S-2 ( $\delta^{34}S_{V-CDT} = 22.58 \pm .39$ ) and IAEA-S-3 ( $\delta^{34}S_{V-CDT} = -32.18 \pm .45$ ) were analyzing repeatedly as unknown samples to verify the accuracy of the calibration method.

*In-situ* sulfur isotope analyses of sphalerite were performed on a Neptune Plus MC-ICP-MS (Thermo Fisher Scientific, Bremen, Germany) equipped with a RESolution S155 193 nm laser ablation system at the Guangzhou Tuoyan Testing Technology Co. LTD. The single spot ablation mode was used. Then the large spot size (24  $\mu m$ ) and slow pulse frequency (6 Hz) were used to avoid the down hole fractionation effect. The laser fluence was kept constant at 4 J/cm<sup>2</sup>. In order to reduce the influence of matrix effect on the test results, sulfide similar to the sample matrix were used as standard samples in the analysis process, and the standard - sample - standard crossing method was used for quality discrimination correction. All data reduction of S isotope ratios was conducted using “Iso-Compass” software (Zhang et al., 2020). All data reduction for the MC-ICP-MS analysis of S isotope ratios was conducted using “Iso-Compass” software (Zhang et al., 2020).

## 6 Result

### 6.1 Laser Raman spectral characteristics of bitumen

Bitumen samples from Xujiashai, Xiaocaoba and Maoping were analyzed by laser Raman, and their maturity parameters are indicated in Table 1. The multiple spot analyses of different areas in the bitumen samples provided similar spectra (“n” means the

numbers of spectra) (Figure 8). The quantitative Raman measurement showed that the Raman spectral characteristics of bitumen in the three places were similar. The specific characteristics indicated that the energy intensity values of Defect-Activated peaks (D peak) were lower, with Raman shifts of the bitumen in Xujiashai, Xiaocaoba and Maoping measuring 1,341 to 1,357 cm<sup>-1</sup>, 1,335 to 1,347 cm<sup>-1</sup> and 1,341 to 1,346 cm<sup>-1</sup>, respectively, and the full width at half maxima of the D peak (FWHM-D) from 229 to 264 cm<sup>-1</sup>, 191 to 256 cm<sup>-1</sup> and 223 to 245 cm<sup>-1</sup>, respectively. The energy intensity of the G peak was relatively high, with Raman shifts from 1,580 to 1,596 cm<sup>-1</sup>, 1,589 to 1,599 cm<sup>-1</sup> and 1,591 to 1,594 cm<sup>-1</sup>, respectively, and the full width at half maxima of the G peak (FWHM-G) from 74 to 89 cm<sup>-1</sup>, 58 to 78 cm<sup>-1</sup> and 60 to 68 cm<sup>-1</sup>, respectively. The Raman spectral characteristics of our bitumen samples were consistent with the pyrobitumen characteristics described by Liu et al. (2013).

Many studies have confirmed that there is a great linear relationship between the characteristic parameter  $R_3$  of the laser Raman spectrum of organic matter and its recorded maximum temperature (T/°C) (Beysac et al., 2002; Rahl et al., 2005). Therefore, the Raman spectral characteristics of carbon-containing organic matter can be used as a geological thermometer. Based on equation of Rahl et al. (2005), we calculated the maximum temperature recorded by bitumen, see, Eq. 1 below:

$$T(^{\circ}C) = 737.3 + 320.9 \times R_1 - 1067 \times R_3 - 80.638 \times R_1^2 \quad (1)$$

where T = estimated temperature;  $R_1 = Dh/Gh$  (Dh refers to the peak height D and Gh refers to the peak height G);  $R_3 = AD/(AD + AG)$  (AD refers to area of the D peak, AG refers to area of the G peak).

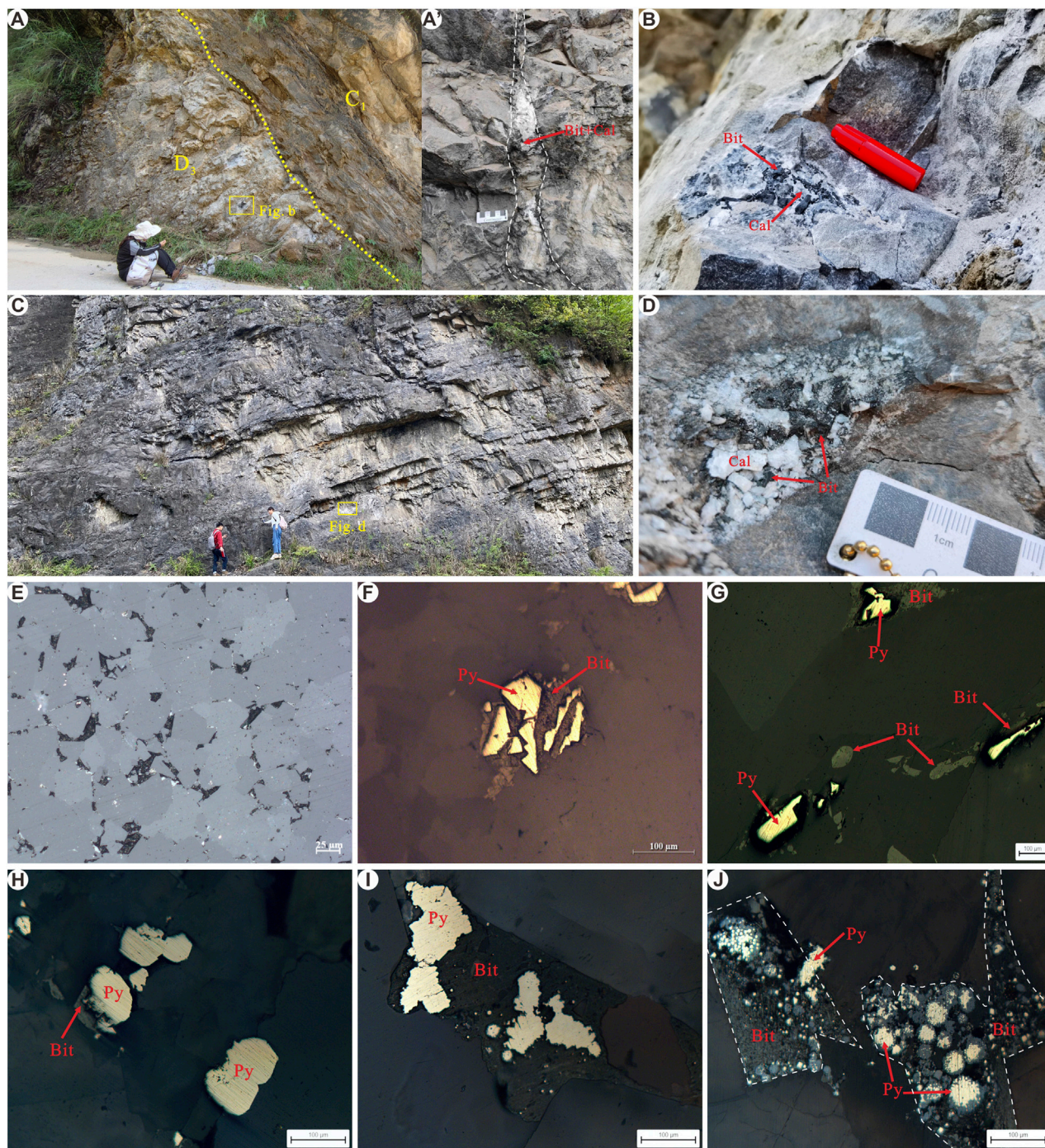


**FIGURE 7**

(A) The outcrop of the Xujiazhai paleo-oil reservoir. Bitumen in the Devonian; (A') Bitumen produced in the Carboniferous, found at 30 m northeast of point "A." Bitumen is distributed in the calcite veins or incorporated in the calcite grains in the form of fine granular or water droplets; (B) The bitumen of a water droplet in the upper Devonian intergrown with calcite (Xujiazhai); (C) Xinchang profile outcrop of the Xiaocaoba paleo-oil reservoir; (D) Bitumen distributed in dissolution voids of upper Devonian dolomite and intergrown with recrystallized calcite (Xiaocaoba); (E) The intercrystalline pores of dolomite mostly filled with bitumen (Xujiazhai); (F,G) The irregular pyrite associated with bitumen in the Xujiazhai paleo-oil reservoir; (H–J) The semi-hedral pyrite associated with bitumen in the Xiaocaoba paleo-oil reservoir (H), irregular (I) and fine-grained aggregate strawberry (J). The strawberry pyrite partially oxidized to grayish goethite. Py, pyrite; Cal, calcite; Bit, bitumen.

The calculated result indicated that bitumen samples from Xujiazhai, Maoping and Xiaocaoba were 176°C–236°C, 173°C–226°C, and 149°C–160°C, respectively. The calculated the maximum temperatures recorded for bitumen were consistent

with the temperature of ore-forming fluid (102°C–247°C, Han et al., 2007; Wang, 2018), indicated that solid bitumen may be formed by cracking of paleo-oil reservoir under thermal action of ore-forming fluid.

**TABLE 1** Relevant parameters of the Raman spectra of bitumen for estimated temperatures and estimated organic maturity.

Sample	D	G	G-D	FWHM-D	FWHM-G	Dh	Gh	R <sub>1</sub>	AD	AG	R <sub>3</sub>	Ro%	T (°C)
XJZ01	1,351	1,587	235	229	89.3	5,420	6,615	.82	17,56,880	8,84,240	.67	3.71	236
XJZ02	1,348	1,583	236	251	83.5	7,530	9,106	.83	26,53,200	11,41,950	.7	3.72	202
XJZ03	1,350	1,584	234	262	84.3	4,832	5,489	.88	17,64,930	6,94,711	.72	3.79	192
XJZ04	1,346	1,580	234	258	84.6	4,744	5,401	.88	17,13,060	6,86,321	.71	3.78	195
XJZ05	1,341	1,586	245	263	77.1	6,971	8,849	.79	25,53,550	10,28,590	.71	3.68	179
XJZ06	1,346	1,585	239	263	80.8	8,564	10,683	0.8	31,45,780	12,97,970	.71	3.69	187
XJZ07	1,341	1,585	244	252	74	9,286	11,344	.82	32,76,100	12,66,750	.72	3.71	176
XJZ08	1,344	1,588	244	263	76	4,841	6,248	.77	17,75,380	7,16,329	.71	3.66	177
XJZ09	1,347	1,585	239	264	81	6,206	7,341	.85	22,81,890	8,94,083	.72	3.74	184
XJZ10	1,357	1,596	239	245	83	7,618	9,804	.78	26,26,550	12,22,070	.68	3.66	210
MPHD-1	1,339	1,595	256	229	62.3	10,323	15,817	.65	33,51,210	14,96,160	.69	3.52	175
MPHD-2	1,339	1,594	254	233	64.8	9,740	14,826	.66	32,08,790	14,56,920	.69	3.52	179
MPHD-3	1,347	1,589	241	256	78.3	5,258	6,615	.79	18,80,930	7,79,913	.71	3.69	187
MPHD-4	1,340	1,599	259	219	57.9	15,050	24,787	.61	46,84,890	21,85,720	.68	3.47	175
MPHD-5	1,335	1,596	262	220	58.6	6,721	10,993	.61	21,03,000	9,80,743	.68	3.47	176
MPHD-6	1,342	1,592	250	238	69.1	6,649	9,168	.73	22,31,920	9,58,408	0.7	3.6	181
MPHD-7	1,343	1,594	251	227	68.4	6,496	9,835	.66	20,94,470	10,17,370	.67	3.53	196
MPHD-8	1,342	1,595	253	228	65	6,048	9,317	.65	19,53,030	9,18,299	.68	3.52	186
MPHD-9	1,341	1,592	251	191	63	6,061	10,149	0.6	16,67,240	9,71,256	.63	3.46	226
MPHD-10	1,337	1,593	256	235	64	6,778	10,136	.67	22,53,040	9,84,455	0.7	3.54	173
XC-1	1,345	1,591	246	242	65.9	7,890	11,670	.68	30,02,480	12,08,920	.71	3.55	157
XC-2	1,343	1,594	251	236	59.7	12,686	20,912	.61	47,02,760	19,59,790	.71	3.47	149
XC-3	1,342	1,593	250	231	62.2	7,115	10,683	.67	25,83,040	10,44,560	.71	3.54	155
XC-4	1,343	1,593	249	236	62.7	9,228	14,197	.65	34,21,940	13,98,210	.71	3.52	154
XC-5	1,346	1,591	245	245	68	8,235	11,701	0.7	31,64,860	12,49,070	.72	3.58	158
XC-6	1,343	1,592	249	232	64.8	7,202	10,305	0.7	26,24,930	10,48,800	.71	3.57	160
XC-7	1,343	1,593	250	235	61.6	7,241	11,089	.65	26,77,400	10,73,590	.71	3.52	151
XC-8	1,343	1,593	251	236	61.4	7,172	11,097	.65	26,55,820	10,69,900	.71	3.51	150
XC-9	1,341	1,593	252	223	61.1	6,935	10,274	.68	24,25,910	9,85,250	.71	3.55	158
XC-10	1,344	1,593	249	241	62.8	10,411	16,129	.65	39,41,230	15,90,180	.71	3.51	151

Note: D, D peak; G, G peak; FWHM-D, full width at half-maximum of D peak; FWHM-G, full width at half-maximum of G peak; Dh, peak height of D; Gh, peak height of G; AD, area of the D peak; AG, area of the G peak; R<sub>1</sub> = Dh/Gh; R<sub>3</sub> = AD/(AD + AG); Ro% refers to  $\rho_{mc}Ro\%$ .

### 6.2 Trace elements contents of bitumen

The metal element contents of bitumen in Xujiashai and Maoping are shown in Table 2. The bitumen samples ranged widely, from 134 to 2,94,000 ppm Zn, 15.3 to 11,700 ppm Pb. The Pb and Zn contents in the bitumen samples were .77–477 times and 1.89–4,141 times, respectively, the Clarke values of the crust (Figure 9). In addition, recyclable metal elements such as Ag, Cd, and Sb were also relatively enriched in bitumen, while Ge and Bi were relatively depleted (Figure 9).

### 6.3 *In-situ* sulfur isotope of sulfide associated with bitumen

*In-situ* sulfur isotope analysis results are shown in Table 3. The results indicated that the  $\delta^{34}S$  value of the pyrite associated with bitumen in the paleo-oil reservoir varied widely (–27.7 to 19.2‰) and could be divided into two groups: –27.7 to –5.7‰ and 0.9 to 19.2‰ (Figures 10A,B). The  $\delta^{34}S$  values of pyrite and sphalerite associated with bitumen in the Maoping deposit ranged from 3.8‰ to 13.9‰ and 11.6‰ to 12.4‰, respectively (Table 3).

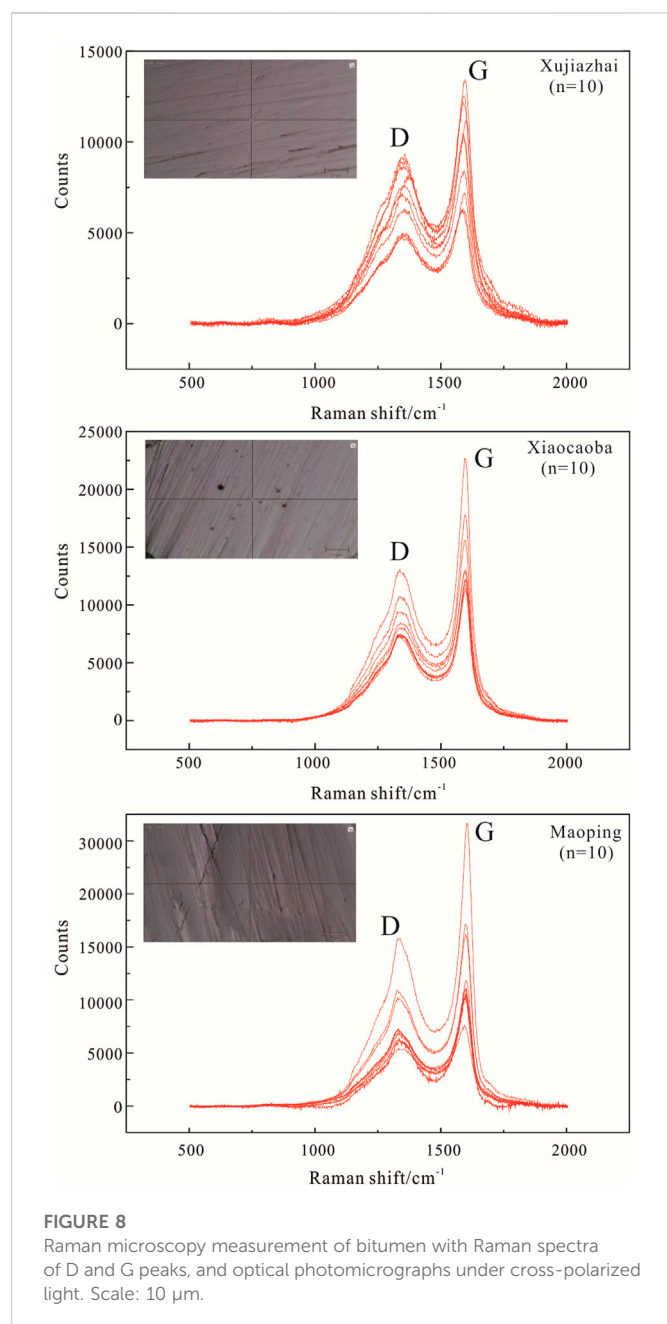


**FIGURE 8**  
Raman microscopy measurement of bitumen with Raman spectra of D and G peaks, and optical photomicrographs under cross-polarized light. Scale: 10  $\mu\text{m}$ .

## 7 Discussion

### 7.1 Maturity of bitumen based on Raman spectrum

The maturity of reservoir bitumen is a key parameter for the inversion of crude oil cracking process. However, the study of bitumen maturity using reflectance is affected by the sample preparation, particle size, and the strong optical anisotropy, which lead to the problem of strong data dispersion and multiple solutions in the test results (Si et al., 2022). Raman spectrum is a scattering that is basically unaffected by the above factors. Studies on different types of vitrinite coal, rock, kerogen bitumen, and other samples have shown that the Raman spectrum of solid organic matter is correlated with the degree of thermal evolution (Xiao et al., 2020; Tian et al., 2021). Many

scholars have calculated the maturity of bitumen by Raman spectra characteristics and obtained good results (Duan et al., 2002; Liu et al., 2013; Zhang et al., 2013; Wang et al., 2015). Using diagram of bitumen maturity (Zhang et al., 2013; Figure 11), all bitumen samples fell in the over mature area, indicating that these bitumens were over mature.

The reflectance of bitumen was determined by laser Raman characteristic peaks (peak height) using equation of Liu et al. (2013), which is equivalent to vitrinite reflectance that can reflect different maturation grades and the surface optical properties of samples; see, Eq. 2 below:

$$R_{\text{mc}}\text{Ro}(\%) = 1.1659 \times R_1 + 2.7588 \quad (2)$$

where  $R_{\text{mc}}\text{Ro}\%$  refers to the Raman reflectance using Raman parameters;  $R_1$ , see Eq. 1. This equation is mainly applicable to over mature solid organic matter (Liu et al., 2013), which corresponded to our samples.

In the samples, the equivalent reflectivity ( $R_{\text{mc}}\text{Ro}\%$ ) values of bitumen from Xujiazhai, Maoping, and Xiaocaoba were 3.66%–3.79% ( $n = 10$ , average 3.72%), 3.47%–3.58% ( $n = 10$ , average 3.53%), and 3.46%–3.69% ( $n = 10$ , average 3.53%), respectively. These values were consistent with the measured results of the reflectance of solid bitumen in the Xiaocaoba paleo-oil reservoir (3.38%–3.47%, Zhang et al., 2017), proving that the calculation of bitumen reflectance by Raman spectrum parameters is reliable. Bitumen samples from the three places had similar and high reflectance, indicating that the studied bitumen belonged to the same paleo-oil reservoir cracking products and had the same burial-thermal evolution history (Bao et al., 2016).

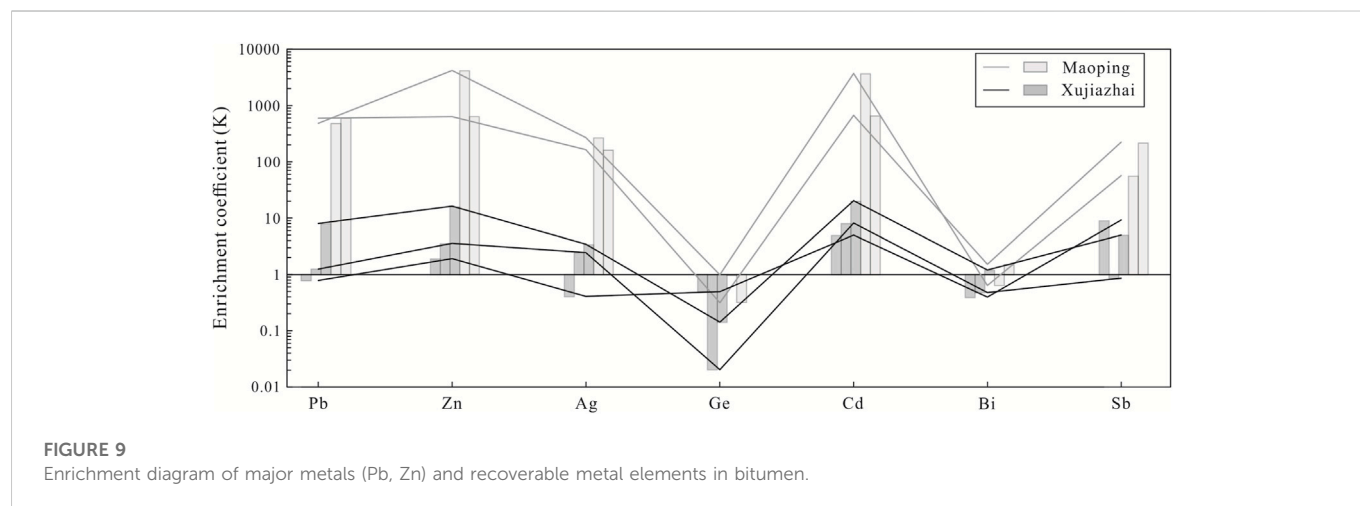
### 7.2 Source of ore-forming metals of the Maoping Pb-Zn deposit

In generally, ore-hosting sedimentary rocks of Sinian to Middle Permian, basements rocks (Proterozoic Kunyang and Huili Group) and Late Permian Emeishan continental flood basalts are collectively regarded as three potential metal source rocks for Pb-Zn deposits in the northeast Yunnan region (Liu and Lin 1999; Huang et al., 2004; Tan et al., 2017; Tan et al., 2019; Zhou et al., 2018; He et al., 2020; Wu et al., 2021). Based on Pb and Zn isotopes, the ore-forming metal elements of the Maoping Pb-Zn deposit was mainly derived from crystalline basement and ore-hosting carbonate rocks far from the mining area rather than Emeishan continental flood (Tan et al., 2017; Tan et al., 2019; He et al., 2020; Wu et al., 2021). Beside, it has been widely accepted that 230–200 Ma is the main period of lead-zinc deposit formation in this area (Tan et al., 2017; Tan et al., 2019; He et al., 2020), whereas the Emeishan basalts were formed at 260 Ma ago (Zhou et al., 2002). Hence, Emeishan basalt has weak capacity to provide metallic material. In addition, black mudstone also is considered to an important metal source for Pb-Zn deposits in the area, such as Jinshachang lead-zinc deposit (Zhou et al., 2015). Recent studies show that for the MVT lead-zinc deposits which have bitumen with abundant Pb and Zn elements, the parent rocks of bitumen (source rocks) are also considered to be one of the metallogenic metal sources, e.g., Nanmushu and Wusihe Pb-Zn deposits in Sichuan Basin (Huang et al., 2021; Wang et al., 2022).

Experiments have shown that petroleum can carry zinc and/or lead (Girodano, 1985; Peabody and Einaudi, 1992; Sanz-Robinson and Williams-Jones, 2019). Within a certain maturity range, crude oil can be an important carrier of Pb-Zn and other metals and an important

TABLE 2 Analysis results of trace elements in bitumen (ppm).

Sample name	Pb	Zn	Ag	Ge	Cd	Bi	Sb
MPHD-1	9,540	2,94,000	13.3	1.55	357	.08	11.2
MPHD-2	11,700	44,200	8.06	.55	64.9	.19	43.9
XJZ-1	158	1,170	.17	.22	1.92	.15	.98
XJZ-2	24.5	249	.12	.03	.79	.06	.17
XJZ-3	15.3	134	.02	.79	.48	.05	1.82



component of the ore-forming fluid (Peabody and Einaudi, 1992; Manning and Gize, 1993; Zhuang and Lu, 1996). The average Zn and Pb contents worldwide in crude oil are .2–.5 ppm and .5–6 ppm, respectively (Manning and Gize, 1993), while the maximum Pb and Zn contents in Venezuela Boscan crude oil are 21 ppm and 160 ppm, respectively (Yang, 1997). The Pb–Zn contents of crude oil are similar to or higher than the Pb (2.0 ppm) and Zn (1.3 ppm) contents required for the MVT Pb–Zn ore-forming fluids (Sverjensky, 1984). Thus, crude oil can be a component of ore-forming fluid. The bitumen from the Xujiazhai paleo-oil reservoir and Maoping deposit had a fertile content of Pb (15.3–11,700 ppm) and Zn (134–2,94,000 ppm), which were .77–477 times and 1.89–4,141 times the Clark values of the crust, respectively (Table 2). This is common in MVT deposits worldwide. For example, the content of solid bitumen Zn in MVT deposits in North America and Spain is generally 10–1,000 ppm (Curiale, 1993). The content of Zn in bitumen from the Huayuan lead–zinc mine in Hunan province of China is 200–20,248 ppm (Liu et al., 1999). The contents of Pb and Zn in bitumen in the Nanmushu lead–zinc deposit in northwest Sichuan Basin are 15.6–2,600 ppm (average 461 ppm,  $n = 10$ , Huang et al., 2021) and 129.9–>10,000 ppm (average > 4,123 ppm,  $n = 10$ , Huang et al., 2021); in the Xuequ lead–zinc deposit in southwestern Sichuan Basin, they are 20–287 ppm and 15–5,370 ppm (Tan et al., 2021); and they are 15.3–161.6 ppm and 129.9–1171.5 ppm in the Mayuan lead–zinc deposit in northern Sichuan Basin (Tan et al., 2021). These values are much higher than the Pb and Zn content in Pb and Zn ore-forming fluids (2.0 and 1.3 ppm, respectively; Sverjensky, 1984), suggesting that not only oil plays the role of metal element transport medium, but also that the hydrocarbon fluid may be the ore-forming fluid, and the

metal elements and oil have the same characteristics in source, transport and aggregation (Tan et al., 2021). It is well known that with the increase in the burial depth of source rock, organic matter in source rock begins to mature and forms crude oil. If the metal elements in the source rock migrate together with crude oil from the source rock, this will enrich the ore-forming metal elements in oil (Huang et al., 2021). Thus, whether the bitumen from the reservoir is rich in metal elements becomes a direct way to test this possibility. The high Zn concentrations is likely resulted by sphalerite inclusions in bitumen based on extremely strong positive relationship between Zn and Cd. However, no apparent sphalerite inclusions were observed in bitumen based on optical microscope. Oil contains not only metallic elements but also small amounts of sulfur (Girodano, 1985; Ohmoto and Goldhaber, 1997), a small amount of sphalerite may be formed during the oil accumulation. This indicates the sphalerite of micron-nanometer scale size may exist in the oil reservoir, which is significantly different from the millimeter-scale size metal sulfides in the orebody, suggesting that the metal sulfides in the ore body should have formed at a different time than the micron-scale sulfides in the bitumen (Huang et al., 2021), that is, the microdot sulfide should be formed during the oil accumulation. In addition, the bitumen of Xujiazhai far away from the mining area also contains rich Pb and Zn content (Table 2). Hence, the enrichment of Pb and Zn elements in bitumen and the laboratory experiment with crude oil dissolving high concentrations of Pb and Zn (Sanz-Robinson and Williams-Jones, 2019) indirectly suggest that source rocks (the parent rocks of bitumen) could be potential sources of metallogenetic elements in lead–zinc deposits.

**TABLE 3 Sulfur isotope of sulfides associated with bitumen in paleo-oil reservoirs and the Maoping deposit.**

Location	Sample name	Sample description	$\delta^{34}\text{S}$ (‰)
Xiaocaoba	XC-1py-1	Subhedral granular pyrite associated with bitumen in the paleo-oil reservoir	-25.5
	XC-1py-2		-25.6
	XC-1py-3		-25.5
	XC-1py-4		-25.0
	XC-1py-5		-25.2
	XC-1py-6		-24.7
	XC-3py-1	Xenomorphic granular pyrite associated with bitumen in the paleo-oil reservoir	-22.7
	XC-3py-2		14.8
	XC-3py-3		-8.1
	XC-3py-4		0.9
	XC-3py-5		19.2
	XC-3py-6		-5.7
Xujiazhai	XJZ-6py-1	Subhedral granular pyrite associated with bitumen in the paleo-oil reservoir	-23.9
	XJZ-6py-2		-27.7
	XJZ-6py-3		-27.6
	XJZ-6py-4		-26.2
	XJZ-6py-5		-23.7
	XJZ-6py-6		-22.9
Maoping	MPHD-6py-1	Euhedral granular pyrite associated with bitumen in the Maoping deposit	13.9
	MPHD-6py-2		13.7
	MPHD-6py-3		10.8
	MPHD-6py-4		3.8
	MPHD-6py-5		9.7
	MPHD-6py-6		11.5
	MPHD-6sp-1	Xenomorphic sphalerite associated with bitumen in the Maoping deposit	12.1
	MPHD-6sp-2		11.6
	MPHD-6sp-3		12.0
	MPHD-6sp-4		12.4
MPHD-6sp-5	12.0		

The NYGD widely distributed source rocks (Wufeng-Longmaxi Formation and Qiongzhusi Formation) which have affluent Pb and Zn content [Zn 30–658 ppm, (Feng et al., 2021); averages: Pb 214 ppm, Zn 256 ppm, (Xiong, 2010); Zn 264 ppm, (Xia, 2016); Pb 493 ppm, Zn 1,656 ppm, (Cheng et al., 2019; Cheng et al., 2020)]. The enrichment of Pb and Zn elements in kerogen can reach 10 or even 100 times that of source rocks (Wang et al., 1996; Wang et al., 1997; Yang et al., 2015), and the maximum of Pb and Zn elements in kerogen is  $n \times 10^{-3}$  (Liu and Jin, 1995), indicating that crude oil can pre-enrich metal elements through the process from original organisms to kerogen in source rocks (Cao et al., 2012), thus enabling source rocks to become the initial ore source beds. In this process, metal elements enrichment is actually related

to surrounding rock geological environment, that is, the organism formed element enrichment through the interaction with the surrounding rock geological environment (Cao et al., 2012). We also note that the regional source rocks are similar to the basement rocks on the REE geochemical characteristics (Figures 12A–F). It indicates the provenance of the source rocks may be from the basement rocks. In fact, many studies likewise showed that the source rocks of the Wufeng-Longmaxi Formation and the Cambrian Qiongzhusi Formation originated from the Huili Group and Kunyang Group of Kangdian uplift (He et al., 2021; Liu et al., 2021). During the sedimentary period of the source rocks, the basement rocks have been exposed to weathering and denudation, providing Pb and Zn elements to source rocks

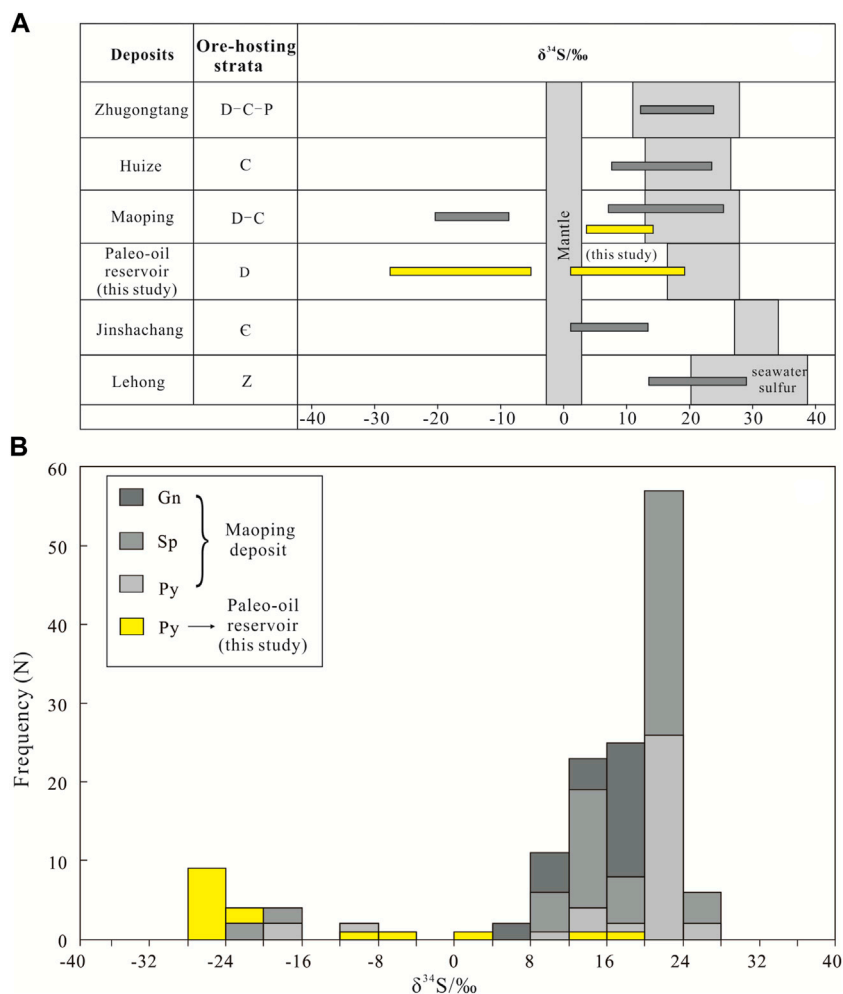


**FIGURE 10**

(A) Comparison of S isotopic compositions between the Pb–Zn deposits hosted in different strata ages of the NYGD, the sulfide of the paleo-oil reservoir, and the seawater and mantle-derived sulfur; (B) Histogram of the sulfur isotope frequency distribution of sulfide in the Maoping Pb–Zn deposit and paleo-oil reservoir. Data sources: mantle-derived sulfur is from (Chaussidon and Lorand, 1990); seawater sulfur is from (Claypool et al., 1980); and ore deposit sulfur is from (Han et al., 2007; Zhang et al., 2014; Zhou et al., 2015; Ren et al., 2018; Wang, 2018; Tan et al., 2019; He et al., 2020; Xiang et al., 2020; Wei et al., 2021a).

(Huang et al., 2021). In addition, if the hydrothermal fluids extracted ore-forming materials from the basement rocks to form metal-rich fluids and flowed into black mudstone along the contemporaneous fault or flowed through the black mudstone layer, the metal elements would be adsorbed due to the strong adsorption capacity of organic matter (e.g., kerogen) to metal ions, led to enrichment of lead and zinc content in source rocks. Therefore, no matter which way the metal elements in the source rocks are enriched, the Pb–Zn rich source rocks have the potential to serve as the ore source bed. During the process of the deep burial of the source rocks, the ore-forming metal elements are separated from the source rocks. As the transporting agents of metallogenic metal elements, petroleum carrying affluent ore-forming metal elements migrated from the source rocks to the trap and accumulated to form metal-rich paleo-oil reservoirs, so the oils have the potential to contribute to the available metal elements for mineralization (Wang et al., 2022). In summary, we believe that these source rocks in the area may directly provide some metal materials for the Maoping Pb–Zn deposit through the

transport by oil, while the basement rocks are the original source of metal materials.

### 7.3 Generation of the H<sub>2</sub>S and metallogenic process in Maoping Pb–Zn deposit

The  $\delta^{34}\text{S}$  value of sulfide in the Pb–Zn deposits in the NYGD was positive, which was related to thermochemical sulfate reduction (TSR) (Ren et al., 2018; Wang, 2018; Tan et al., 2019; Yang et al., 2019; Wei et al., 2021b). In addition to a large positive value, the sulfide in the Maoping Pb–Zn deposit also had a large negative  $\delta^{34}\text{S}$  value (–20.4‰ to –8.7‰, Tan et al., 2019), interpreted as bacterial sulfate reduction (BSR). It is well known that an open system and favorable temperature are necessary for BSR (Furusaka, 1961; Orr, 1977; Machel, 2001; Wing and Halevy, 2014). BSR typically occurs at temperatures lower than 100°C, although it occurs in some cases up to 120°C (Jørgensen et al., 1992; Basuki et al., 2008). A relatively broad range from 102°C to 247°C can represent the metallogenic temperature of the Maoping Pb–Zn deposit (Han et al., 2007; Wang, 2018).

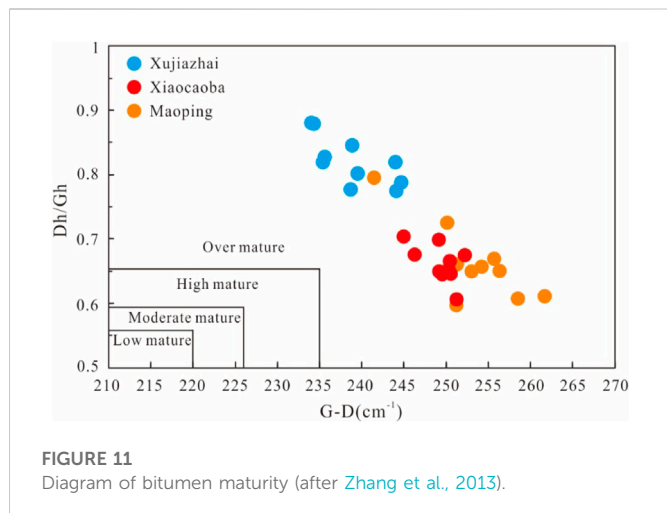


**FIGURE 11**  
Diagram of bitumen maturity (after Zhang et al., 2013).

These temperatures are not suitable for BSR. Tan et al. (2019) interpreted this large negative  $\delta^{34}\text{S}$  value as the BSR process at low temperature before mineralization, and the formation of  $\text{H}_2\text{S}$  in the Maoping deposit was local reduction. In fact, in this case, because much larger fractionation of up to 71‰ of sulfur isotopes is possible with BSR (Goldhaber and Kaplan, 1975; Canfield and Teske, 1996),  $\text{H}_2\text{S}$  may be generated at a site different from

that of mineralization, such as the Jinding Pb–Zn deposit in China, which was interpreted as BSR phenomena occurring prior to or during migration of the hydrocarbons into the reservoir to form the paleo-oil reservoir (Lan et al., 2021). Plentiful bitumen in the Maoping deposit provided a possible explanation for this case. In addition, the temperatures suitable for BSR ( $<100^\circ\text{C}$ – $120^\circ\text{C}$ , Jørgensen et al., 1992; Basuki et al., 2008) partly overlapped with the temperature range of petroleum maturation/expulsion ( $80^\circ\text{C}$ – $160^\circ\text{C}$ ). Therefore, the large negative  $\delta^{34}\text{S}$  value of reduced sulfur in the Maoping deposit can also be interpreted as: BSR phenomena could occur in prior to migration of the hydrocarbons into the reservoir or low mature oil stage in paleo-oil reservoir; slight  $\text{H}_2\text{S}_{\text{BSR}}$  combined with metal ions from the Maoping deposit to form early fine-grained strawberry aggregate pyrite and/or gelatinous sphalerite.

In this study, the  $\delta^{34}\text{S}$  values of pyrite associated with bitumen in the paleo-oil reservoir were similar to those of sulfide in the Maoping deposit and had a broad range ( $-27.7\text{‰}$  to  $19.2\text{‰}$ ), which was significantly different from mantle-derived magmatic sulfur ( $-3.0\text{‰}$  to  $+3.0\text{‰}$ ) (Figure 10A; Chaussidon and Lorand, 1990), although slight values are close to that of mantle-derived sulfur. Beside, because of the study area absence of regional magmatic activity during the metallogenic period, the source of mantle-derived sulfur can be excluded. Most likely, hence sulfate reduction is a major source of sulfur.

At present, it is generally believed that there are two main reduction mechanisms for the conversion of sulfate to reduced sulfur in oil and gas

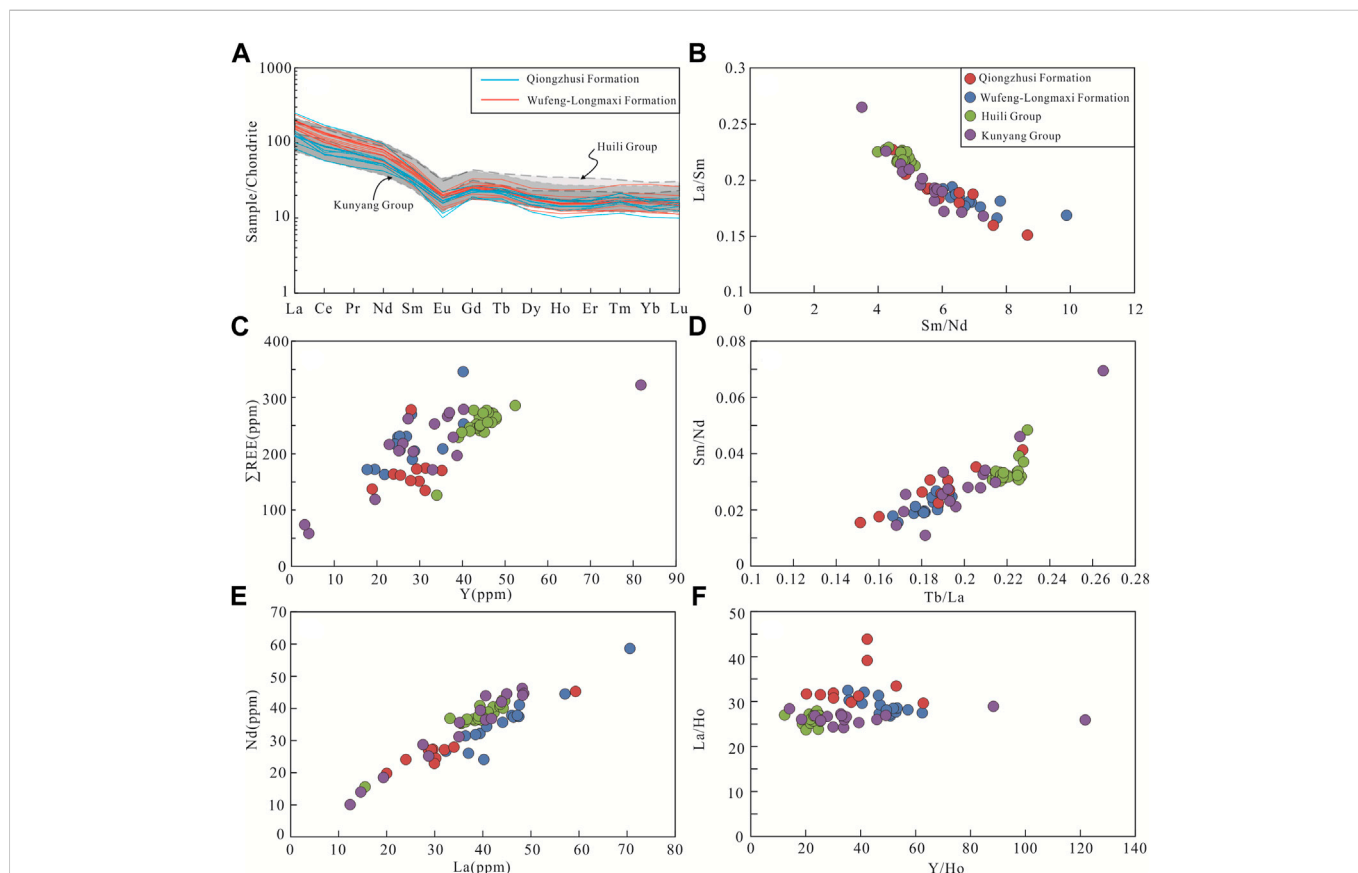


**FIGURE 12**  
Rare Earth element comparison between the Qiongzhusi Formation and Wufeng-Longmaxi Formation source rocks and the basement rocks of Kuyang group and Huili group. (A) Chondrite-normalized REE patterns; (B) Y vs.  $\Sigma\text{REE}$ ; (C) La vs. Nd; (D) Sm/Nd vs. La/Sm; (E) Tb/La vs. Sm/Nd; (F) Y/Ho vs. La/Ho. Data of source rocks are from Xia, 2016; Data of basement rocks are from Yin, 2015; Ji et al., 2016.

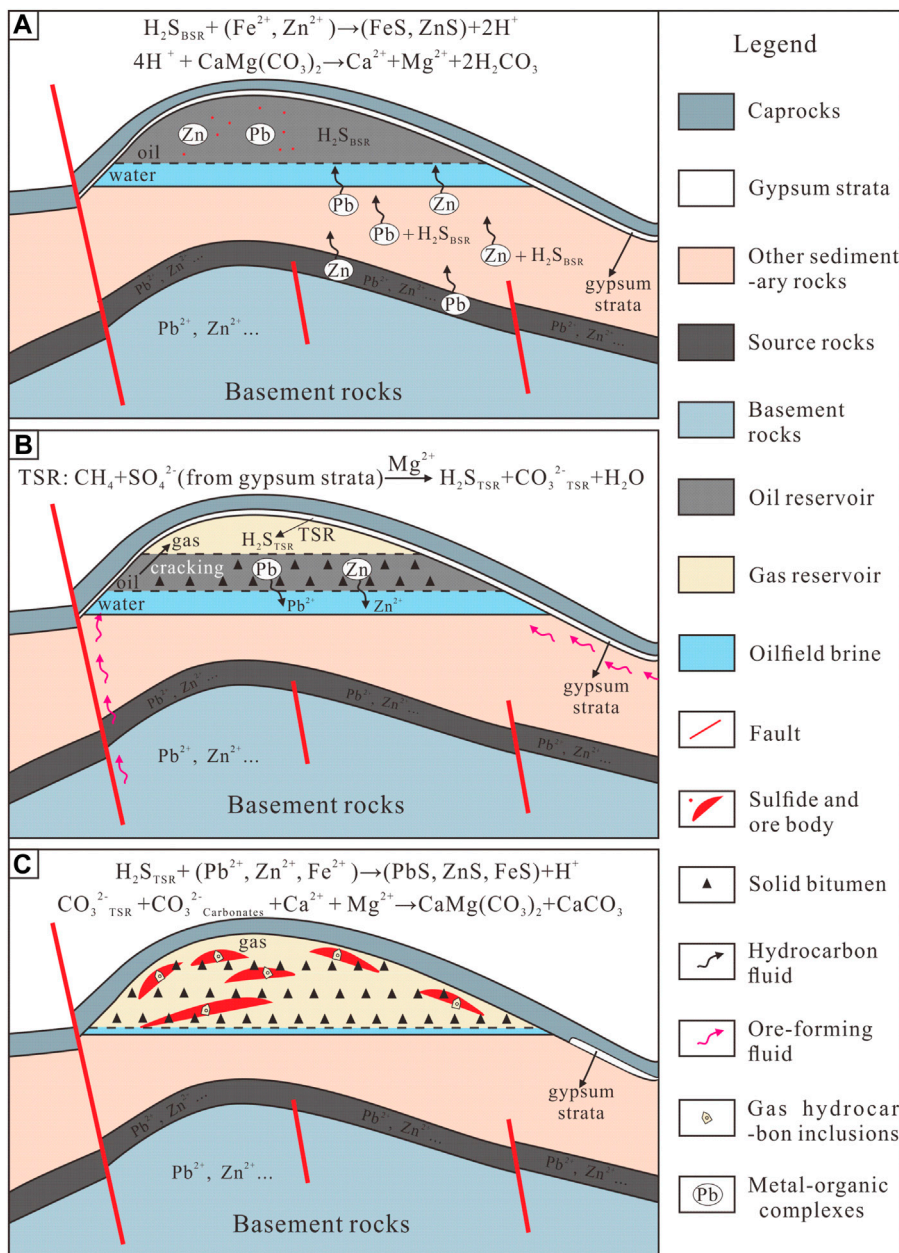
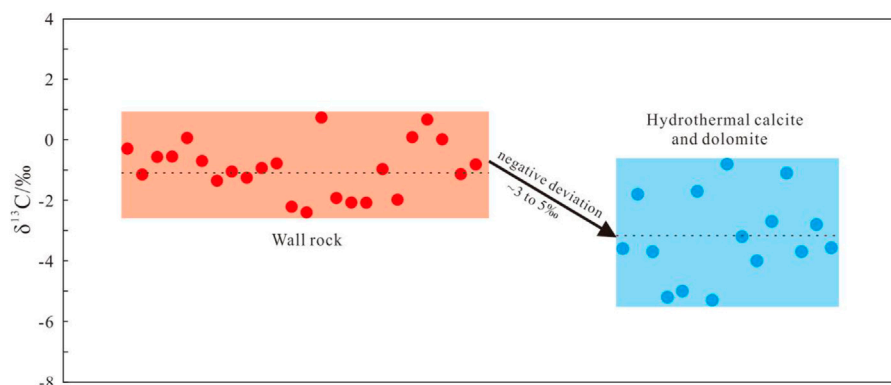


FIGURE 13

Schematic metallogenic model for the Maoping Pb-Zn deposit, showing the genetic relationship between oil and gas accumulation and lead-zinc mineralization. (A) Petroleum carries lead-zinc metals into the reservoir; (B) Paleo-oil reservoir cracking into paleo-gas reservoir and the organic complexes in petroleum are decoupled from the metals. Hydrocarbon organic gas acted as a reducing agent and transformed  $SO_4^{2-}$  in the gypsum strata into  $H_2S_{TSR}$  through TSR. (C) A large amount of sulfide with heavy sulfur isotope value precipitates.

reservoirs, namely: BSR and TSR (Basuki et al., 2008; Luo et al., 2015; Cheng et al., 2021). The depletion of the  $\delta^{34}S$  values of the pyrite in the paleo-oil reservoir ( $-27.7\%$  to  $-5.7\%$ ) was similar to the sulfides with large negative values in the Maoping deposit ( $-20.4\%$  to  $-8.7\%$ , Tan et al., 2019). As mentioned above, these lower values reduced sulfur may have been also provided by BSR during oil formation, migration and accumulation. The aggregates of framboidal pyrite in the bitumen from the paleo-oil reservoir (Figure 7) are also good evidence that sulfate-reducing microbes were present; pyrite framboids are thought to be a consequence of sulfate-reducing microbial activity (Schoonen, 2004; Picard et al., 2018).

Generally during TSR, significant sulfur isotopic fractionation between parent sulfate and produced sulfide [ $\Delta(\delta^{34}S_{sulfate} - \delta^{34}S_{sulfide})$ ] is about 20‰ at a temperature of 100°C, about 15‰ at 150°C, and about 10‰ at 200°C (Machel et al., 1995). The  $\delta^{34}S$  value of the Zaige Formation gypsum strata in the periphery of the Maoping lead-zinc mining area ranged from 21.9‰ to 25.9‰, with an average of 23.6‰ (Ren et al., 2018). According to the maximum temperature of hydrocarbon fluid calculated by the Raman spectral characteristics of bitumen (149°C–236°C, Table 1) and the temperatures of ore-forming fluids recorded in the fluid inclusions of the carbonate minerals



**FIGURE 14**

C isotope correlation between hydrothermal carbonate minerals and wall rocks in Maoping lead-zinc deposit (Data are from Han et al., 2007; Wei, 2011; He et al., 2020).

from the deposit ( $102^{\circ}\text{C}$ – $247^{\circ}\text{C}$ , Han et al., 2007; Wang, 2018), the sulfur isotopic fractionation caused by TSR reaction was estimated to be about  $10\text{‰}$ – $20\text{‰}$  and the sulfur isotopic value of the resulting sulfide  $1.9\text{‰}$ – $15.9\text{‰}$ , which was fully consistent with the pyrite ( $3.8\text{‰}$ – $13.9\text{‰}$ ) and sphalerite ( $11.6\text{‰}$ – $12.4\text{‰}$ ) associated with bitumen in the Maoping deposit and pyrite ( $.9\text{‰}$ – $19.2\text{‰}$ ) in the paleo-oil reservoir (Table 3). Although experimental simulations have proved that it is difficult for simple  $\text{CaSO}_4$  system to initiate TSR reaction at medium and low temperature, but when the temperature is up to  $550^{\circ}\text{C}$  or  $\text{Mg}^{2+}$  is added, the occurrence of TSR will be easier (Hoffmann and Steinfatt, 1993; Yue et al., 2003; Tang et al., 2005). Obviously, this temperature is higher than the metallogenic temperature of Maoping Pb-Zn deposit. While  $\text{Mg}^{2+}$  could be generated by the reaction of  $\text{H}^+$  produced in the early sulfide precipitation process with the wall rocks (dolomite) (as described later). These results indicated that the reduced sulfur of the pyrite ( $.9\text{‰}$ – $19.2\text{‰}$ ) with the heavy sulfur isotope in the paleo-oil reservoir was mainly due to the TSR action of marine evaporates gypsum strata in the reservoir.

As mentioned above, BSR and TSR processes were recorded by the pyrite in the paleo-oil reservoir, which was consistent with the mechanism of reduced sulfur formation in the Maoping deposit. In addition, sulfides in the paleo-oil reservoir and Maoping deposit had similar sulfur isotope distribution characteristics (Figures 10A,B). Therefore, we believe that the formation and evolution of the paleo-oil reservoirs were closely related to the metallogenic process of the Maoping lead-zinc deposit and that they had the same source of sulfur. A large amount of bitumen with high maturity and organic gases (e.g.,  $\text{CH}_4$  and  $\text{C}_2\text{H}_6$ ) exists in the fluid inclusions of the Maoping deposit, indicating that the paleo-gas reservoir formed by the evolution of the paleo-oil reservoir was involved in mineralization. The specific metallogenic process may be as follows:

1) BSR phenomena can occur during oil formation, migration and accumulation; a small amount of  $\text{H}_2\text{S}_{\text{BSR}}$  combined with metal ions in paleo-oil reservoir and deposit to form early subhedral granular, xenomorphic granular, fine-grained strawberry aggregate pyrite and/or gelatinous sphalerite (Figure 13A). At this stage,  $\text{H}^+$  can be released in the process of sulfide precipitation, then  $\text{H}^+$  dissolved dolomite produces a large amount of  $\text{Mg}^{2+}$  (Wu et al., 2013b).

- 2) Due to the injection of ore-forming hydrothermal fluids which could be carrying some metallic material, the oil occurs by thermal cracking led to the oil reservoir began to convert to the gas reservoir and generate pyrolysis bitumen. When the pyrolysis bitumen is formed, these micron-sized sphalerite formed during oil accumulation are wrapped in the pyrolysis bitumen. Afterwards, hydrocarbon organic gas acted as a reducing agent and transformed  $\text{SO}_4^{2-}$  in the Zaige Formation gypsum strata on the periphery of the Maoping lead-zinc mining area into  $\text{H}_2\text{S}_{\text{TSR}}$  through TSR, providing reduced sulfur and creating environmental conditions for mineralization. During or after the transformation of the paleo-oil reservoir into the paleo-gas reservoir, the decoupling of the metals-organic complexes led to metals entering oilfield brine, may have provided the portion of ore metals for mineralization (Huang et al., 2021) (Figure 13B).
- 3) Large-scale sulfide precipitation may have occurred during or after the paleo-oil reservoir cracked into the paleo-gas reservoir (Figure 13C). It is possible that due to the addition of organic carbon, giving rise to the carbon isotopes of hydrothermal carbonate minerals (calcite and dolomite;  $\delta^{13}\text{C} = -5.3$  to  $-0.8\text{‰}$ ; Han et al., 2007; He et al., 2020) in Maoping deposit have a negative deviation of  $\sim 3\text{‰}$  to  $5\text{‰}$  compared with the wall rocks ( $\delta^{13}\text{C} = -2.4$  to  $.8\text{‰}$ ; Wei, 2011) (Figure 14).

## 8 Conclusion

- 1) The bitumen in the Xujiashai, Xiaocaoba paleo-oil reservoirs and Maoping deposit has a high degree of evolution. They are formed by cracking of petroleum.
- 2) The bitumen in the Xujiashai paleo-oil reservoir and Maoping deposit has an abundant Pb and Zn content, indicating petroleum liquids may act as transporting agents for ore metals, carrying them to sites where mineralization may take place. The source rocks in the northern Yunnan-Guizhou depression may have provided not only the oil for paleo-oil/gas reservoirs, but also a portion of ore metals for the Pb-Zn mineralization.
- 3) The formation and evolution of paleo-oil reservoirs are closely related to the metallogenic process of the Maoping lead-zinc deposit, and their sulfides have the same sulfur source and formation mechanism as reduced sulfur. Massive sulfide

precipitation may have occurred during or after the paleo-oil reservoir cracked into the paleo-gas reservoir.

## Data availability statement

The original contributions presented in the study are included in the article/supplementary material, further inquiries can be directed to the corresponding authors.

## Author contributions

Conceptualization, YH; Investigation, SX, YH, JZ, YP, QZ and ZP; Data curation, SX; Writing—original draft preparation, SX; Writing—review and editing, SX, YH and YC; Supervision, YH; Funding acquisition, YH. All authors have read and agreed to the published version of the manuscript.

## Funding

This research was supported by the National Natural Science Foundation of China (41672073).

## References

- Bao, J. P., Si, C. S., Jiang, X. C., Zhang, R. H., Zhu, C. S., Huang, L., et al. (2016). Study on origin and source of solid bitumen from the Xiaocaoba paleo-reservoir in the northern Guizhou Depression. *Geochim.* 45, 315–328. doi:10.3969/j.issn.0379-1726.2016.03.007
- Basuki, N. I., Taylor, B. E., and Spooner, E. T. C. (2008). Sulfur isotope evidence for thermochemical reduction of dissolved sulfate in Mississippi Valley-type zinc-lead mineralization, Bongara area, northern Peru. *Econ. Geol.* 103, 783–799. doi:10.2113/gsecongeo.103.4.783
- Beysac, O., Goffe, B., Chopin, C., and Rouzaud, J. N. (2002). Raman spectra of carbonaceous material in metasediments: A new geothermometer. *J. Metamorph. Geol.* 20, 859–871. doi:10.1046/j.1525-1314.2002.00408.x
- Canfield, D. E., and Teske, A. (1996). Late Proterozoic rise in atmospheric oxygen concentration inferred from phylogenetic and sulphur-isotope studies. *Nature* 382, 127–132. doi:10.1038/382127a0
- Cao, J., Wu, M., Wang, X. L., Hu, W. X., Xiang, B. L., Sun, P. A., et al. (2012). Advances in research of using trace elements of crude oil in oil-source correlation. *Adv. Earth Sci.* 27, 925–936. doi:10.11867/j.issn.1001-8166.2012.09.0925
- Chaussidon, M., and Lorand, J. P. (1990). Sulphur isotope composition of orogenic spinel lherzolite massifs from ariege (North-Eastern pyrenees, France): An ion microprobe study. *Geochim. Cosmochim. Acta* 54, 2835–2846. doi:10.1016/0016-7037(90)90018-G
- Chen, G. P., Xu, G. S., Wang, T. Q., Ma, L., Shi, L. T., and Zheng, C. L. (2008). The relationship between hydrocarbon accumulation and metallization and a discussion on intergrated exploration. *Earth Sci. Front.* 2, 200–206. doi:10.3321/j.issn:1005-2321.2008.02.023
- Chen, Y. R., Jia, G. X., and Dai, T. G. (2002). The role of organic material in metallic mineralization and its application in metal exploration. *Geol. China* 29, 257–262. doi:10.3969/j.issn.1000-3657.2002.03.004
- Cheng, Y., Hu, Y. Z., Li, P. Y., and Lu, P. (2019). The geochemical characteristics of trace elements and paleoenvironmental evolution of black rock series in the lower Cambrian Qiongzhusi Formation from Huize area, eastern Yunnan province. *Contrib. Geol. Mineral. Resour. Res.* 34, 416–422. doi:10.6053/j.issn.1001-1412.2019.03.011
- Cheng, Y., Hu, Y. Z., Wang, D., Wang, P. P., Li, P. Y., and Wang, X. L. (2021). Oil-source rock analysis and metallogenic significance of the palaeo-oil reservoir in the Qinglong antimony deposit, South China. *Ore Geol. Rev.* 137, 104281. doi:10.1016/J.OREGEOREV.2021.104281
- Cheng, Y., Jian, L., Tang, G., and Zhang, C. Y. (2020). Trace element anomaly characteristics and metallogenic significance of the lower cambrian Qiongzhusi Formation from huize area, eastern yunnan province. *Nonfer. Met. Eng.* 10, 90–98. doi:10.3969/j.issn.2095-1744.2020.12.014
- Claypool, G. E., Holser, W. T., Kaplan, I. R., Sakai, H., and Zak, I. (1980). The age curves of sulfur and oxygen isotopes in marine sulfate and their mutual interpretation. *Chem. Geol.* 28, 199–260. doi:10.1016/0009-2541(80)90047-9
- Curiale, J. A. (1993). "Occurrence and significance of metals in solid bitumens: An organic geochemical approach," in *Bitumens in ore deposits*. Editors J. Parnell, H. Kucha, and P. Landais (Berlin, Heidelberg: Springer), 461–474.
- Du, J. P., Ye, X., Shi, S. Y., and Wu, C. (2021). Technological innovation and achievements in the exploration and development of shale gas in complex mountainous areas: A case study of the zhaotong national shale gas demonstration area. *Nat. Gas. Ind.* 41, 41–50. doi:10.3787/j.issn.1000-0976.2021.04.005
- Duan, J. C., Zhuang, X. G., and He, M. C. (2002). Characteristics in laser Raman spectrum of different of coal. *Geol. Sci. Technol. Inf.* 21, 65–68. doi:10.3969/j.issn.1000-7849.2002.02.014
- Fang, W. X., Jia, R. X., Guo, Y. Q., Li, T. C., Wang, L., and Huang, Z. Y. (2016). Hydrocarbon-rich basin fluid with reductibility and metallogenic mechanism for glutenite-type Cu-Pb-Zn-U deposits in the western of tarim basin. *J. Earth Sci. Environ.* 38, 727–752. doi:10.3969/j.issn.1672-6561.2016.06.001
- Feng, W. M., Li, R., Zhao, Z., Yu, Q., Yang, H., Xie, Y., et al. (2021). Boundary definition of Wuéng Formation and Longmaxi Formation in well DD1 and sedimentary environment evolution of northeastern yunnan. *Geol. China* 48, 297–308. doi:10.12029/jgc20210120
- Fu, J., Hu, Z. C., Zhang, W., Yang, L., Liu, Y., Li, M., et al. (2016). *In situ*, sulfur isotopes ( $\delta^{34}\text{S}$  and  $\delta^{33}\text{S}$ ) analyses in sulfides and elemental sulfur using high sensitivity cones combined with the addition of nitrogen by Laser Ablation MC-ICP-MS. *Anal. Chim. Acta* 911, 14–26. doi:10.1016/j.aca.2016.01.026
- Furusaka, C. (1961). Sulphate transport and metabolism desulphovibrio desulphuricans. *Nature* 192, 427–429. doi:10.1038/192427a0
- Girodano, T. (1985). A preliminary evaluation of organic ligands and metal-organic complexing in Mississippi Valley-type ore solutions. *Econ. Geol.* 80, 96–106. doi:10.2113/gsecongeo.80.1.96
- Goldhaber, M. B., and Kaplan, I. R. (1975). Controls and consequences of sulfate reduction rates in recent marine sediments. *Soil Sci.* 119, 42–55. doi:10.1097/00010694-197501000-00008
- Gu, X. X., Li, B. H., Dong, S. Y., Xue, C. J., and Fu, S. H. (2012). Hydrocarbon- and ore-bearing basinal fluids: A possible link between gold mineralization and hydrocarbon accumulation in the youjiang basin, south China. *Min. Depos.* 47, 663–682. doi:10.1007/s00126-011-0388-x
- Han, R. S., Zhang, Y., Wang, F., Wu, P., Qiu, W. L., and Li, W. Y. (2019). *Metallogenic mechanism of Germanium-rich Pb-Zn deposit and location forecasting of buried ore in Northeast Yunnan*. Beijing: Science Press, 1–510.
- Han, R. S., Zou, H. J., Hu, B., Hu, Y. Z., and Xue, C. D. (2007). Features of fluid inclusions and sources of ore-forming fluid in the Maoping carbonate-hosted Zn-Pb-(Ag-Ge)

## Acknowledgments

We would like to express special thanks to Hua Zhong, Ce Chen, Jiageng Zuo, and Bo Xu from the Yiliang Chihong Mining Co., LTD., Maoping lead–zinc mine for their generous assistance during fieldwork. We are also deeply grateful to the reviewers for their reviews and constructive suggestions.

## Conflict of interest

The authors declare that the research was conducted in the absence of any commercial or financial relationships that could be construed as a potential conflict of interest.

## Publisher's note

All claims expressed in this article are solely those of the authors and do not necessarily represent those of their affiliated organizations, or those of the publisher, the editors and the reviewers. Any product that may be evaluated in this article, or claim that may be made by its manufacturer, is not guaranteed or endorsed by the publisher.

- deposit, Yunnan, China. *Acta Pet. Sin.* 23, 2109–2118. doi:10.3969/j.issn.1000-0569.2007.09.010
- He, J. W., Xie, Y., Cai, H. M., Liu, J. Q., He, L., and Lu, Y. F. (2021). Geochemical characteristics and geological significance of the silurian Longmaxi Formation shale in yanjin area, southwestern Sichuan Basin. *J. Palaeogeogr. Chin. Ed.* 23, 1174–1191. doi:10.7605/gdxb.2021.06.075
- He, Y. F., Wu, T., Huang, Z. L., Ye, L., Deng, P., and Xiang, Z. (2020). Genesis of the maoping carbonate-hosted Pb–Zn deposit, northeastern yunnan province, China: Evidences from geology and C–O–S–Pb isotopes. *Acta Geochim.* 39, 782–796. doi:10.1007/s11631-020-00424-4
- Hoffmann, G. G., and Steinfatt, I. (1993). “Thermochemical sulfate reduction at steam flooding processes—a chemical approach[C],” in *Proceedings of the 205th ACS national meeting enhanced oil recovery symposium* (Denver: American Chemical Society), 181–184.
- Hu, Z. C., Zhang, W., Liu, Y. S., Gao, S., Li, M., Zong, K. Q., et al. (2015). Wave” signal-smoothing and mercury-removing device for laser ablation quadrupole and multiple collector ICPMS analysis: Application to lead isotope analysis. *Anal. Chem.* 87, 1152–1157. doi:10.1021/ac503749k
- Huang, X. D., Chen, C. H., Lai, X., Song, Z. J., Zhang, Y., Yang, D. P., et al. (2019). The genetic relationship between Pb–Zn deposits and paleo-oil reservoirs in Mayuan, northern Sichuan Basin. *Geol. China* 46, 1547–1555. doi:10.12029/gc20190619
- Huang, Z. L., Chen, J., Han, R. S., Li, W. B., Liu, C. Q., Zhang, Z. L., et al. (2004). *Geochemistry and ore genesis of the huize giant Pb–Zn deposit in yunnan province, China: Discussion on the relationship between the emeishan flood basalts and Pb–Zn mineralization*. Beijing: Geological Publishing House, 1–214.
- Huang, Z., Wang, G. Z., Li, N., Fu, Y. Z., Lei, Q., and Mao, X. L. (2021). Genetic link between Mississippi Valley-Type (MVT) Zn–Pb mineralization and hydrocarbon accumulation in the Namushu, northern margin of Sichuan Basin, SW China. *Geochem.* 81, 125805. doi:10.1016/j.chemer.2021.125805
- Ji, X. X., Zhou, S., Chen, Q., Liu, D. M., and Li, D. W. (2016). Provenance and tectonic setting of the Kunyang group in central yunnan province. *Geol. China* 43, 857–878. doi:10.12029/gc20160312
- Jørgensen, B. B., Isaksen, M. F., and Jannasch, H. W. (1992). Bacterial sulfate reduction above 100°C in deep-sea hydrothermal vent sediments. *Science* 258, 1756–1757. doi:10.1126/science.258.5089.1756
- Kesler, S. E., Jones, H. D., Furman, F. C., Sassen, R., Anderson, W. H., and Kyle, J. R. (1994). Role of crude oil in the Genesis of Mississippi Valley-type deposits: Evidence from the Cincinnati arch. *Arch. Geol.* 22, 609–612. doi:10.1130/0091-7613(1994)022<0609:rocoit>2.3.co;2
- Kozłowski, A. (1995). Origin of Zn–Pb ores in the olkusz and chrzanów districts: A model based on fluid inclusion. *Acta Geol. Pol.* 45, 84–141.
- Lan, Q., Hu, R. Z., Bi, X. W., Liu, H., Xiao, J. F., Fu, S. L., et al. (2021). The source of organic matter and its role in producing reduced sulfur for the giant sediment-hosted Jinding zinc-lead deposit, Lanping Basin, Yunnan, southwest China. *Econ. Geol.* 116, 1537–1560. doi:10.5382/econgeo.4838
- Li, F. Y., Gu, X. X., Fu, S. H., and Zhang, M. (2002). The role of organic matter in the Formation of MVT Pb–Zn deposit. *Bull. Min. Pet. Geochem.* 21, 272–276. doi:10.3969/j.issn.1007-2802.2002.04.014
- Li, R. X., Mao, J. W., Zhao, B. S., Chen, B. Y., and Liu, S. W. (2021). A review of the role of hydrocarbon fluid in the ore formation of the MVT Pb–Zn deposit. *Adv. Earth. Sci.* 36, 335–345. doi:10.11867/j.issn.1001-8166.2021.042
- Liang, X., Xu, Z. Y., Zhang, Z., Wang, W. X., Zhang, J. H., Lu, H. L., et al. (2020). Breakthrough of shallow shale gas exploration in Taiyang anticline area and its significance for resource development in Zhaotong, Yunnan province, China. *Pet. Explor. Dev.* 47, 12–29. doi:10.1016/s1876-3804(20)60002-7
- Liang, X., Ye, X., Zhang, J. H., and Shu, H. L. (2011). Reservoir forming conditions and favorable exploration zones of shale gas in the Weixin Sag, Dianqianbei Depression. *Pet. Explor. Dev.* 38, 693–699. doi:10.1016/s1876-3804(12)60004-4
- Lin, Q. (1995). Non-magmatic metallogenic model of petroliferous basin in modern and ancient metallogenic hydrodynamic systems. *Foreign Geol. Sci. Technol.* 3, 12–18.
- Liu, D. H., Xiao, X. M., Tian, H., Min, Y. S., Zhou, Q., Cheng, P., et al. (2013). Sample maturation calculated using Raman spectroscopic parameters for solid organics: Methodology and geological applications. *China Sci. Bull.* 58, 1285–1298. doi:10.1007/s11434-012-5535-y
- Liu, D. M., and Jin, K. L. (1995). Element enrichment of source rock macerals in Tarim Basin. *Coal Geol. Explor.* 5, 19–21.
- Liu, H. C., and Lin, W. D. (1999). *Regularity research of Pb–Zn–Ag ore deposits in northeast Yunnan*. China Kunming, China: Yunnan University Press, 1–468.
- Liu, J. M., Ye, J., Liu, J. J., Tan, J., and Niu, J. J. (2000). Oil accumulation and ore-formation. *Bull. Min. Pet. Geochem.* 19, 164–171. doi:10.3969/j.issn.1007-2802.2000.03.004
- Liu, J. Q., He, L., He, P., Ran, J., He, J. W., and Chen, F. L. (2021). Geochemical characteristics and significance of the Qiongzhusi Formation on the eastern margin of the ancient kangding-yunnan Land: Taking the xinchanggou section of zhaoyang district, zhaotong city, yunnan province as an example. *Acta Sedimentol. Sin.* 39, 1305–1319. doi:10.14027/j.issn.1000-0550.2020.052
- Liu, W. J., Zheng, R. C., Li, Y. L., and Gao, L. (1999). Study of bitumen in the huayuan lead-zinc deposit—organic geochemistry study of MVT lead-zinc deposit. *Acta Sedim. Sin.* 17, 19–23.
- Liu, W. J., and Zheng, R. C. (2000). Thermochemical reduction of sulfate and Huayuan lead-zinc deposit. *Sci. China (Series D Earth Sci.)* 30, 456–464. doi:10.3969/j.issn.1674-7240.2000.05.002
- Liu, Y., Hu, K., Han, C. S., and Sun, Z. H. (2016). The characteristics of organic matter and its relationship with the formation of Carlin-type gold deposits in Southwest Guizhou Province. *Geochem.* 45, 281–302. doi:10.3969/j.issn.0379-1726.2016.03.005
- Luo, H. Y., Liu, W. H., Wang, W. C., Tenger Fan, M., and Han, Y. (2015). H. Discovery of the mineralogical evidence of the thermochemical sulfate reduction in black shale. *Bull. Mineral. Pet. Geochem.* 34, 330–333. doi:10.3969/j.issn.1007-2802.2015.02.014
- Machel, H. G. (2001). Bacterial and thermochemical sulfate reduction in diagenetic settings—Old and new insights. *Sediment. Geol.* 140, 143–175. doi:10.1016/S0037-0738(00)00176-7
- Machel, H. G., Krouse, H. R., and Sassen, R. (1995). Products and distinguishing criteria of bacterial and thermochemical sulfate reduction. *Appl. Geochem.* 10, 373–389. doi:10.1016/0883-2927(95)00008-8
- Manning, D. A. C., and Gize, A. P. (1993). “The role of organic matter in ore transport processes,” in *Organic geochemistry: Principles and applications*. Editors M. H. Engels and S. A. Macko (New York: Plenum Press), 547–563.
- Ohmoto, H., and Goldhaber, B. (1997). Sulphur and carbon isotopes. *Geochem. Hydrothermal Ore Deposits* 174, 517–600.
- Orr, W. L. (1977). “Geologic and geochemical controls on the distribution of hydrogen sulfide in natural gas,” in *Advances in organic geochemistry* (Enadisma, Madrid: Springer), 571–597.
- Peabody, C. E., and Einaudi, M. T. (1992). Origin of petroleum and mercury in the Culver-Baer cinnabar deposit, Mayacmas District, California. *Econ. Geol. Bull. Soc. Econ. Geol.* 87, 1078–1103. doi:10.2113/gsecongeo.87.4.1078
- Picard, A., Gartman, A., Clarke, D. R., and Girguis, P. R. (2018). Sulfate reducing bacteria influence the nucleation and growth of mackinawite and greigite. *Geochim. Cosmochim. Acta* 220, 367–384. doi:10.1016/j.gca.2017.10.006
- Potts, P. J., and Kane, J. S. (2005). International association of geoanalysts certificate of analysis: Certified reference material OU-6 (penrhyn slate). *Geostand. Geoanal. Res.* 29, 233–236. doi:10.1111/j.1751-908x.2005.tb00895.x
- Püttmann, W., Hagemann, H. W., Merz, C., and Speczik, S. (1988). Influence of organic material on mineralization processes in the Permian Kupferschiefer formation, Poland. *Pol. Org. Geochem.* 13, 357–363. doi:10.1016/0146-6380(88)90056-3
- Rahl, J. M., AnderSon, K. M., Brandon, M. T., and Fassoulas, C. (2005). Raman spectroscopic carbonaceous material thermometry of low-grade metamorphic rocks: Calibration and application to tectonic exhumation in Crete, Greece. *Earth Planet. Sc. Lett.* 240, 339–354. doi:10.1016/j.epsl.2005.09.055
- Ren, S. L. (2018). Effect of gypsum salt rocks in the mineralization of huize and maoping Pb–Zn deposits in yunnan: Constraints from sulfur isotopic compositions. Master’s thesis. Beijing: China University of Geosciences, 1–60.
- Ren, S. L., Li, Y. H., Zeng, P. S., Qiu, W. L., Fan, C. F., and Hu, G. Y. (2018). Effect of sulfate evaporate salt layer in mineralization of the huize and maoping lead-zinc deposits in yunnan: Evidence from sulfur isotope. *Acta Geol. Sin.* 92, 1041–1055. doi:10.3969/j.issn.0001-5717.2018.05.010
- Rieger, A., Schwark, L., Cisternas, M. E., and Miller, H. (2008). Genesis and evolution of bitumen in Lower Cretaceous lavas and implications for stratabound copper deposits, North Chile. *Econ. Geol.* 103, 387–404. doi:10.2113/gsecongeo.103.2.387
- Saintilan, N. J., Spangenberg, J. E., Chiaradia, M., Chelle-Michou, C., Stephens, M. B., and Fontboté, L. (2019). Petroleum as source and carrier of metals in epigenetic sediment-hosted mineralization. *Sci. Rep.-UK.* 9, 8283–8287. doi:10.1038/s41598-019-44770-7
- Sanz-Robinson, J., and Williams-Jones, A. E. (2019). Zinc solubility, speciation and deposition: A role for liquid hydrocarbons as ore fluids for Mississippi valley type Zn–Pb deposits. *Chem. Geol.* 520, 60–68. doi:10.1016/j.chemgeo.2019.05.002
- Schoonen, M. A. (2004). Mechanisms of sedimentary pyrite formation: Special paper of the geological society of America. *Front. Earth Sci.* 379, 117–134. doi:10.3389/feart.2020.588310
- Si, S. H., Yang, Z. H., Chen, Y. Z., Song, L. J., Shang, X. Q., Er, C., et al. (2022). Thermal evolution characteristics and discrimination of reservoir bitumen based on Raman spectroscopy. *Spectrosc. Spect. Anal.* 42, 783–787. doi:10.3964/j.issn.1000-0593(2022)03-0783-05
- Sicree, A. A., and Barnes, H. L. (1996). Upper Mississippi Valley district ore fluid model: The role of organic complexes. *Ore Geol. Rev.* 11, 105–131. doi:10.1016/0169-1368(95)00018-6
- Spangenberg, J. E., and Herlec, U. (2006). Hydrocarbon biomarkers in the Topla-Mežica zinc-lead deposits, northern Karavanke/Drau Range, Slovenia: Paleoenvironment at the site of ore formation. *Econ. Geol.* 101, 997–1021. doi:10.2113/gsecongeo.101.5.997
- Sverjensky, D. A. (1984). Oil field brines as ore-forming solutions. *Econ. Geol.* 79, 23–37. doi:10.2113/gsecongeo.79.1.23
- Tan, S. C., Zhou, J. X., Li, B., and Zhao, J. X. (2017). *In situ* Pb and bulk Sr isotope analysis of the yinchanggou Pb–Zn deposit in sichuan province (SW China): Constraints

- on the origin and evolution of hydrothermal fluids. *Ore Geol. Rev.* 91, 432–443. doi:10.1016/j.oregeorev.2017.09.012
- Tan, S. C., Zhou, J. X., Luo, K., Xiang, Z. Z., He, X. H., and Zhang, Y. H. (2019). The sources of ore-forming elements of the Maoping large-scale Pb-Zn deposit, Yunnan Province: Constraints from *in-situ* S and Pb isotopes. *Acta Pet. Sin.* 35, 3461–3476. doi:10.18654/1000-0569/2019.11.13
- Tan, T., Wang, G. Z., Peng, H. L., Huang, Z., and Zuo, L. (2021). Origin of ore-forming metal elements of MVT type Pb-Zn deposit in Dengying formation, Sichuan basin. *J. Min. Pet.* 41, 68–79. doi:10.19719/j.cnki.1001-6872.2021.04.07
- Tang, Y. C., Ellis, G. S., Zhang, T. W., and Jin, Y. B. (2005). Effect of aqueous chemistry on the thermal stability of hydrocarbons in petroleum reservoirs. *Geochim. Cosmochim. Ac.* 69, A559.
- Thompson, M., Potts, P. J., Kane, J. S., and Wilson, S. (2000). GeoPT5. An international proficiency test for analytical geochemistry laboratories - report on round 5. *Geostand. Geoanal. Res.* 24, E1–E28. doi:10.1111/j.1751-908X.2000.tb00592.x
- Tian, J. Z., Chen, Y., Hou, F. X., Tian, R., Zhang, H., Wang, Y. J., et al. (2021). Raman spectroscopic characteristics of reservoir bitumen and its constrain on stages of hydrocarbon accumulation — take yangshuiwu buried hill of jizhong depression as an example. *Spectrosc. Spect. Anal.* 41, 131–135. doi:10.3964/j.issn.1000-0593(2021)01-0131-05
- Wang, G., Lei, Q., Huang, Z., Liu, G., Fu, Y., Li, N., et al. (2022). Genetic relationship between Mississippi Valley-type Pb-Zn mineralization and hydrocarbon accumulation in the Wushihe deposits, southwestern margin of the Sichuan Basin, China. *Minerals* 12, 1447. doi:10.3390/min12111447
- Wang, M. L., Xiao, X. M., Wei, Q., and Zhou, Q. (2015). Thermal maturation of solid bitumen in shale as revealed by Raman spectroscopy. *Nat. Gas. Geosci.* 26, 1712–1718. doi:10.11764/j.issn.1672-1926.2015.09.1712
- Wang, P. J., Li, H., Chang, P., and Wang, D. P. (1997). Sequential analysis of blackshales and its application to biomineralization research. *Exp. Pet. Geol.* 19, 382–387. doi:10.1007/BF02951625
- Wang, P. J., Wang, D. P., Chang, P., and Li, H. (1996). Metallic biomineralization of continental black shales. *J. Chang. Univ. Earth Sci.* 26, 47–52. doi:10.13278/j.cnki.jjuese.1996.01.008
- Wang, T. (2018). Study on geology and Genesis of the maoping lead-zinc deposit, zhaotong, yunnan, China. Master's thesis. Chengdu: Chengdu University of Technology, 1–73.
- Wei, A. Y. (2011). Study on alteration-mineralization zonation model of Maoping Pb-Zn deposit group NOL. Master's thesis. Kunming: Kunming University of Science and Technology, 1–137.
- Wei, C., Huang, Z. L., Ye, L., Hu, Y., Santosh, M., Wu, T., et al. (2021a). Genesis of carbonate-hosted Zn-Pb deposits in the Late Indosinian thrust and fold systems: An example of the newly discovered giant Zhugongtang deposit, South China. *J. Asian Earth Sci.* 220, 104914. doi:10.1016/j.jseaes.2021.104914
- Wei, C., Ye, L., Hu, Y. S., Huang, Z. L., Danyushevsky, L., and Wang, H. Y. (2021b). LA-ICP-MS analyses of trace elements in base metal sulfides from carbonate-hosted Zn-Pb deposits, south China: A case study of the maoping deposit. *Ore Geol. Rev.* 130, 103945. doi:10.1016/j.oregeorev.2020.103945
- Williford, K. H., Grice, K., Logan, G. A., Chen, J., and Huston, D. (2011). The molecular and isotopic effects of hydrothermal alteration of organic matter in the Paleoproterozoic McArthur River Pb/Zn/Ag ore deposit. *Earth Planet. Sc. Lett.* 301, 382–392. doi:10.1016/j.epsl.2010.11.029
- Wing, B. A., and Halevy, I. (2014). Intracellular metabolite levels shape sulfur isotope fractionation during microbial sulfate respiration. *P. Natl. Acad. Sci.* 111, 18116–18125. doi:10.1073/pnas.1407502111
- Wu, T., Huang, Z. L., He, Y. F., Yang, M., Fan, H. F., Wei, C., et al. (2021). Metal source and ore-forming process of the maoping carbonate-hosted Pb-Zn deposit in yunnan, SW China: Evidence from deposit geology and sphalerite Pb-Zn-Cd isotopes. *Ore Geol. Rev.* 135, 104214. doi:10.1016/j.oregeorev.2021.104214
- Wu, Y., Zhang, C. Q., Mao, J. W., Ouyang, H. G., and Sun, J. (2013a). The genetic relationship between hydrocarbon systems and Mississippi Valley-type Zn-Pb deposits along the SW margin of Sichuan Basin, China. *Int. Geol. Rev.* 55, 941–957. doi:10.1080/00206814.2012.753177
- Wu, Y., Zhang, C. Q., Mao, J. W., Zhang, W. S., and Wei, C. (2013b). The relationship between oil-gas organic matter and MVT mineralization: A case study of the chipu lead-zinc deposit, sichuan. *Acta Geosci. Sin.* 34, 425–436. doi:10.3975/cagsb.2013.04.05
- Xia, W. (2016). Depositional setting and enrichment mechanism of organic matter of niutitang Formation and Longmaxi Formation in the north of Guizhou province: A case study from well renye-1 and well xiye-1. Master's thesis. Beijing: China University of Geosciences, 1–63.
- Xiang, Z. Z., Zhou, J. X., and Luo, K. (2020). New insights into the multi-layer metallogenesis of carbonated-hosted epigenetic Pb-Zn deposits: A case study of the maoping Pb-Zn deposit, south China. *Ore Geol. Rev.* 122, 103538. doi:10.1016/j.oregeorev.2020.103538
- Xiao, X. M., Zhou, Q., Cheng, P., Sun, J., Liu, D. H., and Tian, H. (2020). Thermal maturation as revealed by micro-Raman spectroscopy of mineral-organic aggregation (MOA) in marine shales with high and over maturities. *Sci. Sin. (Terrae)* 9, 1540–1552. doi:10.1007/s11430-020-9627-2
- Xiong, L. (2010). Geological, geochemical characteristics and metallogenic prediction of Jinniuchang Lead-zinc deposit in Huize, Yunnan province. Master's thesis. Kunming: Kunming University of Science and Technology, 1–79.
- Yang, P., Xie, Y., Wang, Z. J., Du, Q. D., and Liu, J. H. (2012). Geochemical characteristics and oil source correlation of Dengying formation paleo-reservoir in Jinsha. *Geochim* 41, 452–465. doi:10.1007/s11783-011-0280-z
- Yang, Q., Liu, W. H., Zhang, J., Wang, J., and Zhang, X. J. (2019). formation of Pb-Zn deposits in the sichuan-yunnan-guizhou triangle linked to the youjiang foreland basin: Evidence from Rb-Sr age and *in situ* sulfur isotope analysis of the maoping Pb-Zn deposit in northeastern yunnan province, southeast China. *Ore Geol. Rev.* 107, 780–800. doi:10.1016/j.oregeorev.2019.03.022
- Yang, S., Liao, Z. W., Liu, H., Cheng, B., and Xu, J. B. (2015). Geochemical characteristics of trace elements of shales and their residual kerogens from wufeng-longmaxi formations in the qiliiao section, eastern chongqing, China. *Bull. Min. Pet. Geochem.* 34, 1231–1237. doi:10.3969/j.issn.1007-2802.2015.06.015
- Yang, Z. Q. (1997). Modern models for SEDEX deposits and metallogenesis of oil (gas)-bearing thermal brine. *Geol. Min. Resour. South China* 4, 1–7.
- Yin, C. (2015). The geochemistry and tectonic significance of the volcanic rocks in tianbaoshan formation of the Huili group in the Western yangtze block. Master's thesis. Beijing: China University of Geosciences, 1–75.
- Yue, C. T., Li, S. Y., Ding, K. L., and Zhong, N. N. (2003). Simulation experiments on thermochemical sulfate reduction of methane with solid calcium sulfate. *Geochimica* 6, 601–605. doi:10.3321/j.issn:0379-1726.2003.06.012
- Zhang, N., Wang, Z. M., Ju, F. P., Xiao, Z. Y., Fang, Q. F., Zhang, B. S., et al. (2013). Diagenetic bitumen in Ordovician carbonate reservoirs of the northern Tarim Basin. *Acta Pet. Sin.* 34, 225–231. doi:10.7623/syxb201302003
- Zhang, R. H., Si, C. S., Huang, L., Bao, J. P., Ma, L. Q., Wang, P. W., et al. (2017). Genesis and evolution of reservoir bitumen in Xiaocaoaba paleo-oil reservoir, Qianbei Depression. *Pet. Geol. exper.* 39, 99–105. doi:10.11781/syzydz201701099
- Zhang, W., Hu, Z. C., and Liu, Y. S. (2020). Iso-compass: New freeware software for isotopic data reduction of LA-MC-ICP-MS. *J. Anal. At. Spectrom.* 35, 1087–1096. doi:10.1039/D0JA00084A
- Zhang, Y. X., Wu, Y., Tian, G., Shen, L., Zhou, Y. M., Dong, W. W., et al. (2014). Mineralization age and the source of ore-forming material at Lehong Pb-Zn deposit, yunnan province: Constraints from Rb-Sr and S isotopes system. *Acta Mineral. Sin.* 34, 305–311. doi:10.16461/j.cnki.1000-4734.2014.03.002
- Zhou, J. X., Bai, J. H., Huang, Z. L., Zhu, D., Yan, Z. F., and Lv, Z. C. (2015). Geology, isotope geochemistry and geochronology of the Jinshachang carbonate-hosted Pb-Zn deposit, southwest China. *J. Asian Earth Sci.* 98, 272–284. doi:10.1016/j.jseaes.2014.11.024
- Zhou, J. X., Luo, K., Wang, X. C., Wilde, S. A., Wu, T., Huang, Z. L., et al. (2018). Ore Genesis of the fule Pb-Zn deposit and its relationship with the emeishan large igneous province: Evidence from mineralogy, bulk C-O-S and *in situ* S-Pb isotopes. *Gondwana Res.* 54, 161–179. doi:10.1016/j.gr.2017.11.004
- Zhou, M. F., Malpas, J., Song, X. Y., Robinson, P. T., Sun, M., Kennedy, A. K., et al. (2002). A temporal link between the Emeishan large igneous province (SW China) and the end Guadalupian mass extinction. *Earth Planet Sci. Lett.* 196, 113–122. doi:10.1016/S0012-821X(01)00608-2
- Zhuang, H. P., and Lu, J. L. (1996). Organic matter in ore deposits: Characteristics classification and analytical methods. *Adv. Earth Sci.* 11, 372–377. doi:10.11867/j.issn.1001-8166.1996.04.0372
- Zou, H. J., Han, R. S., Hu, B., and Liu, H. (2004). New evidences of origin of metallogenic materials in the maoping Pb-Zn ore deposit, zhaotong, yunnan: R-Factor analysis results of trace elements in NE-extending fractural tectonites. *Geol. Explor.* 40, 43–48. doi:10.3969/j.issn.0495-5331.2004.05.009